ORGANISMAL BIOLOGY

The immune and circulatory systems are functionally integrated across insect evolution

Yan Yan and Julián F. Hillyer*

The immune and circulatory systems of mammals are functionally integrated, as exemplified by the immune function of the spleen and lymph nodes. Similar functional integration exists in the malaria mosquito, *Anopheles gambiae*, as exemplified by the infection-induced aggregation of hemocytes around the heart valves. Whether this is specific to mosquitoes or a general characteristic of insects remained unknown. We analyzed 68 species from 51 families representing 16 orders and found that infection induces the aggregation of hemocytes and pathogens on the heart of insects from all major branches of the class Insecta. An expanded analysis in the holometabolous mosquito, *Aedes aegypti*, and the hemimetabolous bed bug, *Cimex lectularius*, showed that infection induces the aggregation of phagocytic hemocytes on the hearts of distantly related insects, with aggregations mirroring the patterns of hemolymph flow. Therefore, the functional integration of the immune and circulatory systems is conserved across the insect tree of life.

INTRODUCTION

The insect body cavity is a dynamic environment where the insect blood, called hemolymph, constantly and rapidly flows in a manner that bathes all tissues (*1*–*3*). This flow is primarily driven by a dorsal vessel that is structurally divided into an aorta in the thorax and a heart in the abdomen (*4*, *5*). When pathogens invade an adult mosquito and reach its hemocoel, the flow of hemolymph disperses them to all regions of the body (*4*, *6*). Hemolymph flow also circulates immune cells called hemocytes that survey the body for invaders. However, not all hemocytes circulate. Sessile hemocytes exist attached to tissues, yet their distribution is not homogeneous; they concentrate on the outer surface of the dorsal vessel and, specifically, in the regions of the heart that surround the valves, or ostia—locations called the periostial regions (*7*, *8*). Within seconds of infection, these heart-associated hemocytes, called periostial hemocytes, phagocytose circulating pathogens, and soon thereafter, additional hemocytes migrate to the periostial regions and amplify the phagocytosis response (*7*, *9*). Periostial immune responses are advantageous because they occur in areas of high hemolymph flow, placing hemocytes where they are most likely to encounter and destroy pathogens (*9*). Thus, in a manner functionally similar to how the spleen and lymph nodes of vertebrate animals capture pathogens circulating in the blood and lymph (*10*), the function of periostial hemocytes exemplifies the functional integration of the immune and circulatory systems of mosquitoes (Fig. 1).

The biology of periostial hemocytes has only been characterized in the African malaria mosquito, *Anopheles gambiae* (*7*–*9*, *11*, *12*), but hemocytes have also been detected in the lumen of the heart of a stick insect and on the surface of the heart of adult fruit flies and larvae of the greater wax moth (*13*–*17*). Whether the hemocytes of these insects are present near the ostia or whether their response to infection is linked to circulatory currents remained unknown. Hence, we asked whether the functional integration of the immune and circulatory systems is a novel evolutionary trait specific to mosquitoes or a general characteristic of insects. To answer this question, we analyzed 68 species from 51 families representing 16 orders and found that an infection induces the aggregation of hemocytes and pathogens on the heart of insects from all major branches of the class Insecta. Therefore, the functional integration of the immune and circulatory systems is conserved across the insect tree of life.

Department of Biological Sciences, Vanderbilt University, VU Station B 35-1634, Nashville, TN 37235, USA.
*Corresponding author. Email: julian.hillyer@vanderbilt.edu

RESULTS

Infection induces the aggregation of phagocytic hemocytes on the heart of holometabolous and hemimetabolous insects

Having observed the interaction between the immune and circulatory systems in the mosquito, *A. gambiae* (Fig. 1), we conducted a comprehensive analysis of infection-induced hemocyte aggregation on the heart of the yellow fever mosquito, *Aedes aegypti*, and the bed bug, *Cimex lectularius*. These two insect pests diverged ~370 million years ago and have different developmental trajectories: One is holometabolous and the other is hemimetabolous (*18*). Moreover, both are societally important; *A. aegypti* transmits human diseases such as dengue and Zika, and *C. lectularius* is a notorious hematophagous pest.

In preparation for studying the functional integration of the immune and circulatory systems of *A. aegypti* and *C. lectularius*, we quantified how efficiently their hemocytes could be labeled by injecting Vybrant CM-DiI into the hemocoel and examining their perfused hemocytes 20 to 30 min later (fig. S1). Vybrant CM-DiI is a lipophilic dye that, in *A. gambiae*, labels the circulating and sessile hemocytes but does not label the heart, pericardial cells, integument, or any other tissue (*7*–*9*). Moreover, this dye has also been used to label the hemocytes of *A. aegypti* and *Apis mellifera* (Hymenoptera) (*19*, *20*), and therefore, we hypothesized that it could label the hemocytes of any insect. We found that CM-DiI efficiently stains the hemocytes of naïve, injured, and *Escherichia coli*–infected mosquitoes and bed bugs. On average, 84, 83, and 77% of the hemocytes from naïve, injured, and *E. coli*–infected *A. aegypti*, respectively, were stained with CM-DiI. Similarly, 84, 90, and 89% of the hemocytes from naïve, injured, and *E. coli*–infected *C. lectularius*, respectively, were stained with CM-DiI. Fat body and other cells were seldomly stained with CM-DiI, similar to what we have observed for *A. gambiae* (*7*–*9*, *21*).

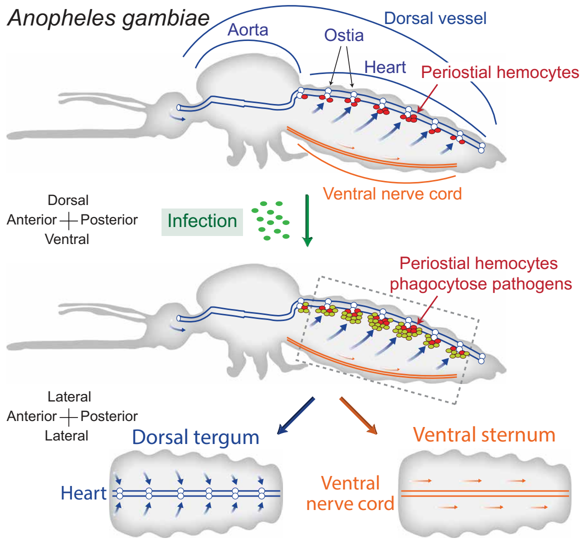

Fig. 1. Diagram that illustrates periostial hemocyte aggregation and the experimental design of this study. The top shows a lateral view of an entire mosquito and marks the position of the dorsal vessel (divided into a thoracic aorta and an abdominal heart), periostial hemocytes (red circles) surrounding the ostia (white circles), and the ventral nerve cord. The middle shows that infection induces the aggregation of additional hemocytes (olive green circles) and the phagocytosis of pathogens around the heart's ostia. The bottom shows a coronal view of the dorsal (tergum) and ventral (sternum) abdomen, which represents how they were visualized and photographed for this study. The arrows mark the direction of hemolymph flow during periods of anterograde heart contractions.

We then assayed for the presence of hemocytes on the heart of mosquitoes and bed bugs by injecting CM-DiI into the hemocoel, bisecting their abdomen, and examining the tubular heart that extends across the dorsal tergum. For *A. aegypti*, approximately 440 hemocytes reside on the heart of a naïve mosquito (Fig. 2A). Injury does not alter the number of periostial hemocytes, but infection results in a 1.7-fold increase in the number of periostial hemocytes. This indicates that, much like occurs in adult *A. gambiae* (*7*), an infection induces the recruitment of additional hemocytes to the heart. A more detailed analysis of the spatial distribution of hemocytes revealed that most hemocytes aggregate in the periostial regions of abdominal segments 3 to 6 (Fig. 2C). Again, this aggregation pattern resembles that of *A. gambiae*, which is advantageous because these middle abdominal segments are the locations that have the swiftest hemolymph flow (*9*). In bed bugs, we observed similar results. Specifically, the average naïve and injured bed bug has 140 and 120 hemocytes on the heart, respectively, but infection induces a twofold increase in the number of heart-associated hemocytes (Fig. 2B). In *C. lectularius*, hemocytes predominantly aggregate in the portions of the heart of abdominal segments 6 and 7 (Fig. 2D). This spatial distribution occurs because this portion of the heart is enlarged and is where the incurrent ostia are located, as evidenced by structural analyses of the heart of other hemipterans, such as the kissing bug, *Rhodnius prolixus* (*22*), and the boxelder bug, *Leptocoris trivittatus* (*23*).

To determine whether the hemocytes that aggregate on the heart are immunologically active, we injected *A. aegypti* and *C. lectularius* with *E. coli* bioparticles conjugated to pHrodo, which is a pH-sensitive dye that only fluoresces in an acidic environment, such as that of the phagolysosome. Therefore, this dye is an efficient marker for phago-

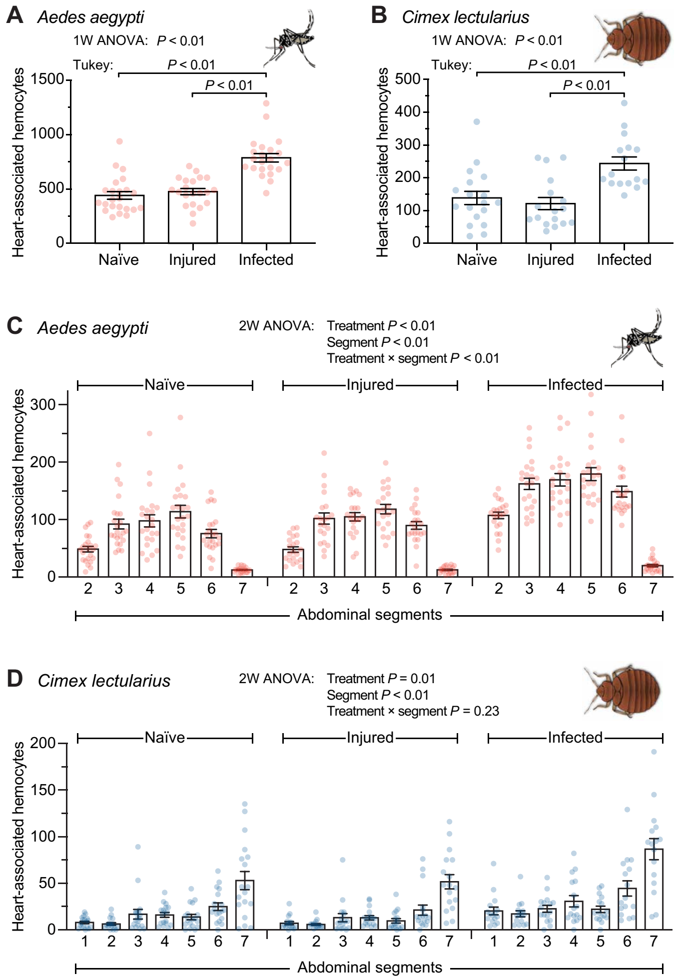

Fig. 2. Infection induces the aggregation of phagocytic hemocytes on the heart of *A. aegypti* and *C. lectularius*. (**A** and **B**) Hemocytes on the heart of naïve, injured, and *E. coli*–infected *A. aegypti* (A) and *C. lectularius* (B). 1W ANOVA, one-way analysis of variance. (**C** and **D**) Spatial distribution of hemocytes along the heart in the different abdominal segments of naïve, injured, and *E. coli*–infected *A. aegypti* (C) and *C. lectularius* (D). Column heights mark the mean, and the whiskers denote the SEM. Each circle represents the number of heart-associated hemocytes in an individual insect. 2W, two-way.

cytosis (*9*). In naïve mosquitoes and bed bugs, no fluorescence was detected, which was expected because no *E. coli* pHrodo was injected. However, when mosquitoes and bed bugs were injected with *E. coli* pHrodo, we detected fluorescence emission soon after injection, and this fluorescence was predominantly in the areas that contain the heart-associated hemocytes (Fig. 3, A and B). Together, these data show that, in both holometabolous and hemimetabolous insects, infection induces the aggregation of hemocytes on the heart and that these hemocytes rapidly phagocytose pathogens that circulate with the hemolymph.

Hemocytes and pathogens aggregate on the hearts of taxonomically diverse insects

Given that periostial hemocyte aggregation occurs in both holometabolous mosquitoes and hemimetabolous bed bugs, we next sought to assess whether periostial immune responses occur throughout the

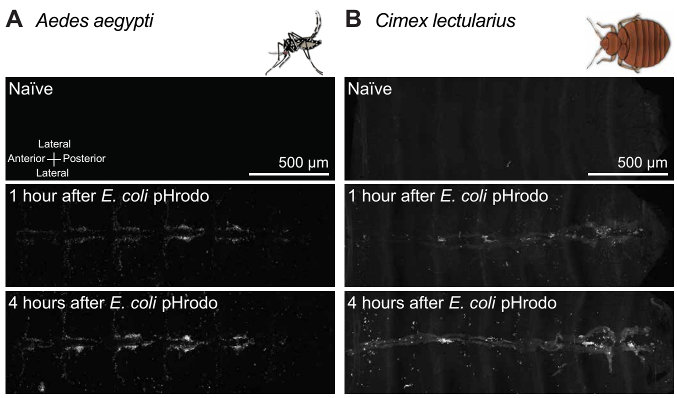

Fig. 3. Heart-associated hemocytes phagocytose bacteria in *A. aegypti* and *C. lectularius*. (**A** and **B**) Phagocytosis of *E. coli* pHrodo by the hemocytes of *A. aegypti* (A) and *C. lectularius* (B). Insects were imaged before injection (naïve; negative control) or at 1 and 4 hours after injection with *E. coli* pHrodo. Fluorescence images show the entire length of the dorsal abdomen of each insect, with the heart extending along the horizontal midline. The heart-associated hemocytes, as well as other sessile hemocytes dispersed throughout the abdomen, actively phagocytose pathogens that circulate with the hemolymph.

class Insecta. We initiated this comprehensive survey by infecting field-collected *Anopheles punctipennis* (Diptera: Anophelinae), *Aedes albopictus* (Diptera: Culicinae), and *Culex* sp. (Diptera: Culicinae) with green fluorescent protein (GFP)–expressing *E. coli* to induce the hemocyte aggregation response. Following hemocyte labeling with CM-DiI, we bisected the mosquito's abdomen and visualized the distribution of hemocytes and pathogens on (i) the tubular heart that extends across the dorsal tergum and (ii) the ventral nerve cord that extends across the ventral sternum (Fig. 1). Both the dorsal and ventral sides of the abdomen were examined because the ventral nerve cord mirrors the location of the heart but is not in a region of high hemolymph flow (*24*). Therefore, if an interaction between the immune and circulatory systems was to exist, hemocytes and pathogens would aggregate on the heart but not on the ventral nerve cord. Much like we found in our *A. gambiae* laboratory colony, in both anopheline and culicine mosquitoes, hemocytes and pathogens aggregate exclusively around the six pairs of cardiac ostia and nowhere else in the tergum or sternum (Fig. 4 and fig. S2).

We next used the same approach to examining members of Pterygota within Holometabola (synonym Endopterygota). In 7 species in Diptera, 2 in Mecoptera, 11 in Lepidoptera, 4 in Trichoptera, 9 in Coleoptera, 1 in Neuroptera, and 6 in Hymenoptera, we once again found that hemocytes and pathogens aggregate along the entire length of the heart in the dorsal abdomen and nowhere else in the body (Fig. 4). Closer examination of the distribution of hemocytes and GFP–*E. coli* revealed two different patterns, but both included hemocyte aggregation around the ostia (Fig. 4 and figs. S2 to S7). In the first pattern, observed in scorpionflies (Mecoptera: Panorpidae), moths (Lepidoptera: Noctuidae), beetles (Coleoptera: Scarabaeidae), and spongillaflies (Neuroptera: Sisyridae), hemocytes and pathogens aggregate in specific foci on the surface of the heart in a manner that is similar to what occurs in the periostial regions of mosquitoes. In the second pattern, observed in house flies (Diptera: Muscidae), butterflies (Lepidoptera: Nymphalidae), caddisflies (Trichoptera: Limnephilidae), honeybees (Hymenoptera: Apidae), and ants (Hymenoptera: Formicidae), hemocytes and pathogens concentrate in specific foci, but they are also sparsely distributed between some of the foci. We failed to detect heart-associated immune responses in the cat flea (Siphonaptera: Pulicidae), where similar amounts of pathogens were present on the dorsal and ventral abdomen. We hypothesize that this is due to variation in circulatory physiology that is associated with the flea's laterally flattened body shape.

Once we found that heart-associated immune responses occur throughout Holometabola, we investigated hemimetabolous species in Neoptera. In six species in Hemiptera, three in Blattodea, one in Phasmatodea, seven in Orthoptera, and two in Plecoptera, we confirmed that hemocyte aggregation only occurs in cardiac tissues and nowhere else in the body (Fig. 4 and figs. S8 to S10). Within Condylognatha, hemocytes and pathogens aggregate in specific foci on the heart of bed bugs (Hemiptera: Cimicidae) and sharpshooters (Hemiptera: Cicadellidae). Moreover, within Polyneoptera, hemocytes and pathogens are both in foci and sparsely distributed between some foci in cockroaches (Blattodea: Blattidae), walking sticks (Phasmatodea: Diapheromeridae), and katydids (Orthoptera: Tettigoniidae). The pattern seen in these Polyneoptera could be because their elaborate dorsal diaphragm provides a larger and more continuous platform for the aggregation of hemocytes (*25*). A completely different pattern occurs in one Polyneoptera—the stonefly (Plecoptera: Perlidae)—where hemocytes and pathogens aggregate only in the heart regions located in the posterior abdominal segments. Although plecopterans have segmental ostia (*25*), it is possible that their distinct pattern of hemocyte aggregation occurs because only the posterior ostia are functional. An alternative explanation is that a reduced dorsal diaphragm reduces the ability of hemocytes to adhere to the heart (*26*).

We then examined another hemimetabolous group: the Paleoptera. In two dragonfly species (Odonata: Libellulidae), hemocytes and pathogens aggregate near the posterior of the heart in a manner that resembles the aggregation pattern in mosquito larvae (Fig. 4 and fig. S10) (*27*). This makes sense given the parallels in circulatory physiology between dragonfly adults and mosquito larvae; odonate adults only have two pairs of abdominal ostia that are located in the posterior of the abdomen, which is similar to how mosquito larvae only allow hemolymph to enter the heart via a posterior incurrent opening (*2*, *25*). Therefore, it appears that their circulatory physiology drives hemocytes and pathogens only to the posterior of the abdomen. A completely different pattern was observed in two mayfly species (Ephemeroptera: Heptageniidae); few hemocytes and pathogens are attached to the abdominal integument, with slightly more hemocytes in the ventral abdomen than in the dorsal abdomen (Fig. 4 and fig. S10). This suggests that heart-associated immune responses do not occur in Ephemeroptera, although ostia are present in all or most abdominal segments (*28*). Because mayfly adults only live ~2 days, we hypothesize that these nonfeeding and short-lived adult insects minimize their investment in immunity in favor of reproduction.

Last, we examined wingless insects that do not undergo metamorphosis (ametabolous) and are the sister group to the Pterygota. Excitingly, infection of silverfish (Zygentoma: Lepismatidae) results in both hemocytes and pathogens distinctively aggregating within the periostial regions—especially toward the posterior end of the heart—although the strength of hemocyte aggregation is less pronounced when compared to more derived insect groups (Fig. 4 and fig. S10). The pattern observed in silverfish mirrors the pattern observed in odonates and plecopterans, raising the possibility that infection-induced hemocyte aggregation at the posterior of the heart

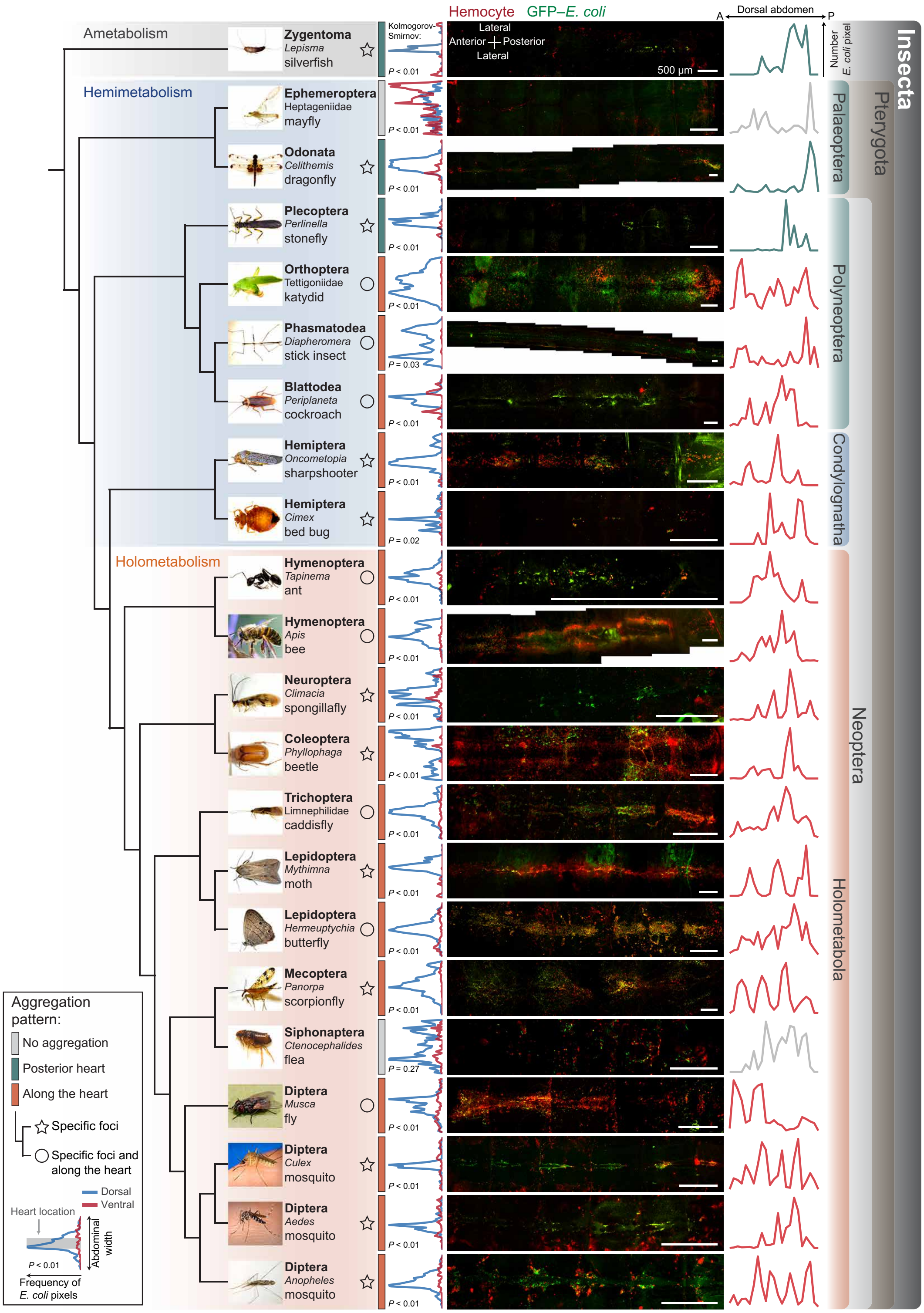

Fig. 4. The heart-associated immune response is a trait shared across the insect tree of life. On the left is a selection of the insects assayed, arranged by insect phylogeny. The fluorescence images near the center show the entire length of the dorsal abdomen of each insect, with the heart extending along the horizontal midline. They show that hemocytes (red) and GFP–*E. coli* (green) aggregate and colocalize on the heart, although more than one pattern was observed (see box for key). To the immediate left of the images are frequency distributions of GFP–*E. coli*–positive pixels along the lateral axis of the dorsal (blue lines) and ventral (red lines) abdomens. To the immediate right of the images are frequency distributions of GFP–*E. coli*–positive pixels along the anterior-posterior axis of the dorsal abdomen. The data show that, except in the mayfly and flea, pathogens aggregate on the heart (blue peaks in the center of the leftmost graphs) and nowhere else. Moreover, peaks in the rightmost graphs show that hemocytes aggregate in the periostial regions along the length of the heart, except in silverfish, dragonflies, and stoneflies, where they aggregate on the periostial regions of the posterior of the heart.

is the pleisiomorphic state. Together, these data show that the immune and circulatory systems are functionally integrated throughout the insect lineage.

DISCUSSION

Substantial efforts have been made to characterize the immunological mechanisms used by insects to fight infection (*29*), yet less attention has been paid to the structural features and functional mechanics of hemolymph propulsion (*4*). Moreover, until recently, how circulatory currents affect immune responses has gone ignored (*4*). This is unexpected because the immune responses of vertebrate animals are intrinsically linked to the flow of blood and lymph (*10*). To address this gap in knowledge, we conducted a comprehensive survey in the class Insecta and, here, show that immunologically active hemocytes are present on the hearts of holometabolous, hemimetabolous, and ametabolous insects and that an infection induces the migration of hemocytes to the periostial regions of the heart, therefore amplifying the immune response.

Although this study uncovered the physiological interaction between two major organ systems, the mechanisms governing this interaction remain mostly unknown. Thioester-containing complement-like proteins and Nimrod family proteins are immune factors that influence the migration of hemocytes to the heart of mosquitoes and fruit flies (*11*, *12*, *16*, *30*). Both of these protein families are encoded in the genomes of diverse insects (*31*, *32*), so their roles in heart-associated responses likely extend beyond Diptera. In addition, a collagen protein that is part of the cardiac extracellular matrix, called Pericardin, facilitates the aggregation of hemocytes on the heart of fruit flies (*13*). Collectively, this means that hemocyte migration to the heart is driven by a combination of immune and cardiac components.

The directional forces of circulatory currents undoubtedly facilitate how hemocytes migrate to the heart. In mosquitoes, hemocytes aggregate in the periostial regions of abdominal segments 2 to 7 and, more precisely, in the locations of the heart that contain the incurrent ostia. Most of these hemocytes aggregate in the periostial regions of the middle abdominal segments, which are the locations of the ostia that receive the most hemolymph flow (*9*). In a similar circulatory pattern, the hemocytes of dragonflies and silverfish aggregate on the posterior of the heart, which is where their incurrent ostia are located (*25*). Given that hemocytes aggregate in areas of high hemolymph flow, it makes sense that allatotropin, which is a neuropeptide that modulates heart rhythmicity (*33*), also alters the number of hemocytes present on the surface of the heart (*19*). In addition, linking immunity and circulation are nitric oxide and lysozymes. They are produced by hemocytes—including periostial hemocytes—to combat bacterial infections, but they also decelerate the insect heart contraction rate (*14*, *29*, *34*, *35*). Nitric oxide also has immune and circulatory functions in vertebrate animals (*36*, *37*). Therefore, the molecular drivers of the physiological interaction between the immune and circulatory systems are undoubtedly complex but are likely conserved across the insect lineage and beyond.

From an evolutionary perspective, insects are hexapods that are nested within a paraphyletic Crustacea, which, collectively, is called the Pancrustacea (*38*). Innovation in the hexapod lineage resulted in the evolution of the tracheal system and the decoupling of hemolymph circulation and gas exchange, which led to a decrease in vasculature and a simplification of the major circulatory organs (*4*, *39*). This simplification resulted in a dorsal vessel that contains ostia and propels hemolymph in three primary ways: (i) bidirectional flow as occurs in Diplura (a noninsect Hexapod) and wingless ametabolous insects, (ii) anterograde flow as occurs in hemimetabolous insects, and (iii) periodic alternation between anterograde and retrograde flow as occurs in holometabolous insects (*4*, *5*). To our knowledge, no studies have investigated how noninsect hexapods (Protura, Collembola, and Diplura) immunologically respond to infection. Regardless, there are many similarities in the immune and circulatory systems of insects and crustaceans (*40*). For example, the primary immune cells in both insects and crustaceans are hemocytes, and the major immune effector pathways are conserved between these two groups (*40*). Moreover, insects and crustaceans both have open circulatory systems that are composed of a hemocoel, hemolymph, and a heart that is located along the dorsal midline (*4*, *5*). Many of the same neuropeptides (e.g., crustacean cardioactive peptide and FMRFamide-like peptides) and neurotransmitters (e.g., serotonin and octopamine) influence cardiac physiology in both animal groups (*4*). Given all these parallels, we hypothesize that the interaction between the circulatory and immune systems extends beyond insects and into noninsect hexapods and crustaceans. Although differences in the architecture of the circulatory systems of insects and crustaceans preclude a direct structural comparison, hemocytes populate the endothelium of the hepatic arterioles of lobsters (*41*), and following an infection, they aggregate on the heart and arterial vessels of prawns and crabs (*42*, *43*). In penaeid shrimp and prawns, heart contractions drive hemolymph into a lymphoid organ, where immune cells destroy circulating pathogens and release humoral immune factors into circulation (*44*, *45*). Therefore, hemocytes in the circulatory structures of decapod crustaceans function in a manner reminiscent of the periostial hemocytes of insects.

In conclusion, insects emerged ~480 million years ago, and Zygentoma diverged from Pterygota ~420 million years ago (*18*). The data presented herein show the conserved association of hemocytes and immune responses on the heart of species that span the entire insect lineage. Therefore, the functional integration of the circulatory and immune systems of insects likely evolved near the origin of the insect lineage or predates the divergence of Insecta from other Pancrustacea.

MATERIALS AND METHODS

A. aegypti and *C. lectularius* colonies

A. aegypti Black Eye Liverpool strain was obtained from the BEI Resources (catalog no. NR-48921, Manassas, VA). Mosquitoes were maintained at 27°C and 75% relative humidity under a 12-hour:12-hour light:dark photoperiod. Adults were maintained in 2.4-liter plastic buckets and fed 10% sucrose. Five-day-old female mosquitoes were used in the experiments.

C. lectularius were obtained from a colony maintained at the Purdue University. Bed bugs were starved for 7 days or more at room temperature before experimental manipulations. A mixture of male and female adult bed bugs of unknown age was used.

Surveyed insects, identification, and phylogeny

Insects were collected in the wild using a sweep net or a light trap or were obtained from established laboratory colonies. Insects were identified to the family or genus level by their external morphology (table S1), and insect phylogeny was inferred from Misof *et al.* (*18*). The following sources were used in the identification of insects: (i) Kaufman Field Guide to Insects of North America (*46*), (ii) bugguide.net,

(iii) and the artificial intelligence model powered by iNaturalist or Seek apps. When identifying insects, consideration was given to their ecology, including geographic distribution, collection site, and time of year. Table S1 details the insects used in this study, including the location and date of collection, the collectors, the infection doses, and other relevant information. Collecting done in state parks or state natural areas was performed pursuant to the State of Tennessee, Department of Environment and Conservation, Division of Natural Areas Scientific Study permit no.: 2019-017. From the time of collection to the time of experimentation, insects were fed a 10% sucrose solution and maintained in a BugDorm (MegaView Science Co., Taiwan) under standard laboratory conditions.

Bacterial growth and insect infection

Tetracycline-resistant, GFP-expressing *E. coli* was grown overnight in Luria-Bertani's (LB) rich nutrient medium in a 37°C shaking incubator (New Brunswick Scientific, Edison, NJ, USA). The absorbance of GFP–*E. coli* cultures was measured spectrophotometrically and normalized to an optical density at 600 nm of 5 before injection. To initiate infections, insects were briefly anesthetized in a tube or Petri dish held over ice and then intrathoracically injected using either a Nanoject III Programmable Nanoliter Injector (Drummond Scientific Company, Broomall, PA, USA) when the injected volume was <2 μl or a calibrated micropipette (Drummond Scientific Company, Broomall, PA, USA) when the injected volume was >2 μl. The injected volume for each insect was normalized to approximately 69 nl per 1 mg of insect weight. The absolute number of *E. coli* injected into each insect was calculated after plating dilutions of the tetracycline-resistant, GFP–*E. coli* culture on an LB plate containing tetracycline and counting the resultant colony-forming units.

A. aegypti and *C. lectularius* CM-DiI hemocyte staining efficiency

Mosquitoes were left unmanipulated (here termed naïve), injured by injecting 69 nl of LB medium or infected by injecting 69 nl of GFP–*E. coli*. One hour later, each mosquito was injected in the thorax with a solution of 67 μM CM-DiI Cell-Labeling Solution (Thermo Fisher Scientific, Waltham, MA, USA) and 1.08 mM Hoechst 33342 (Thermo Fisher Scientific) in phosphate-buffered saline (PBS) until its abdomen became expanded. This protocol specifically labels circulating and sessile hemocytes with CM-DiI and all cell nuclei with Hoechst 33342 (*7*). It was crucial that the staining solution was injected within minutes of its preparation because once the CM-DiI is placed in an aqueous environment, its hemocyte staining effectiveness begins to decrease, approaching 0% after 10 to 15 min of mixing (*7*). At 20 to 30 min later, the hemolymph with circulating hemocytes was perfused by making a small incision at the ventral side of the seventh abdominal segment and then injecting PBS through the thoracic anepisternal cleft. The first five drops of hemolymph that exited the abdomen were collected within a 1-cm-diameter etched ring on a glass slide. The circulating hemocytes were allowed to adhere to the slide for 20 min in a humidity chamber, fixed for 5 min by adding 4% formaldehyde in PBS, and washed three times with PBS for 5 min each, and a coverslip was mounted using Aqua-Poly/Mount (Polysciences, Warrington, PA, USA). A similar protocol was followed for bed bugs, except that the hemolymph was perfused by making a small incision between the sixth and seventh abdominal segments, and PBS was injected through the ventral thorax.

Hemocyte staining efficiency for each insect was measured by examining the first 50 hemocytes that were viewed by simultaneous differential interference contrast (DIC) and fluorescence microscopy on a Nikon 90i compound microscope connected to a Nikon Digital Sight DS-Qi1 monochrome digital camera and Nikon's Advanced Research NIS-Elements software (Nikon, Tokyo, Japan). Cells were considered hemocytes if they had both a nucleus (stained with Hoechst 33342 and seen in the blue channel) and a cell membrane (seen in the DIC channel). Then, hemocytes were considered stained if they had incorporated CM-DiI (seen in the red channel). Hemocytes were distinguished from fat body cells by their substantially smaller size and the absence of large, refractive lipid droplets. Hemocytes were distinguished from the nuclei of lysed cells by examining the DIC channel; nuclei from lysed cells lack a cell membrane. Three independent trials were performed for both *A. aegypti* and *C. lectularius*. Combined, at least 24 mosquitoes and 15 bed bugs were analyzed per treatment group, respectively. Data were analyzed by one-way analysis of variance (ANOVA), followed by Tukey's multiple comparison test (GraphPad Prism, San Diego, CA).

In vivo hemocyte staining and dissection of the dorsal and ventral abdomen

For all insects used in this study, at 1 or 4 hours following infection, hemocytes were stained in vivo using Vybrant CM-DiI as described above. Then, each insect was fixed for 10 min by injecting 16% formaldehyde into the hemocoel until the abdomen began to expand. The head and thorax of each insect were separated from the abdomen using a razor blade, and for insects collected in the wild, the head and thorax were stored in denatured ethanol at −20°C in case further identification was required. The abdomen was then bisected along a coronal plane and immersed in PBS containing 0.1% Triton X-100, and the internal organs were removed. The dorsal abdomen (containing the heart) and the ventral abdomen (containing the ventral nerve cord) were rinsed briefly in PBS and mounted between a glass slide and a coverslip using Aqua-Poly/Mount. Note that some insects were processed at 1 hour after infection, whereas others were processed at 4 hours after infection. For species that were processed at both time points, the results were similar, except that stronger aggregations were sometimes seen at 4 hours.

Visualization and quantification of hemocyte aggregation on the heart of *A. aegypti* and *C. lectularius*

The dissected dorsal abdomens of naïve, injured, and GFP–*E. coli*–infected *A. aegypti* and *C. lectularius* were imaged under bright-field and fluorescence illumination. Z-stacks were acquired using a linear encoded Z-motor, and for image presentation, all images within a stack were combined into a two-dimensional, focused image using the extended depth of focus (EDF) function in NIS-Elements.

The heart-associated hemocytes were counted manually by examining all images within a Z-stack. A cell was counted as a heart-associated hemocyte if it resided near the dorsal vessel and was labeled with both CM-DiI and Hoechst 33342. The heart-associated hemocytes were counted in abdominal segments 2 to 7 in *A. aegypti* and 1 to 7 in *C. lectularius*. The heart-associated hemocytes in segment 1 of *A. aegypti* were not counted because this is the location of the thoracoabdominal ostia. This region is structurally conserved across the dipteran lineage, and its circulatory physiology is different from the other abdominal segments and is a location where few hemocytes are located (*21*, *47*). Three independent trials were performed for both *A. aegypti* and *C. lectularius*. Combined, at least 21 mosquitoes and 16 bed bugs were analyzed per treatment group, respectively. Data were analyzed by one-way ANOVA, followed by Tukey's multiple comparison test.

Visualization of the phagocytic activity of heart-associated hemocytes in *A. aegypti* and *C. lectularius*

E. coli bacterial bioparticles conjugated to pHrodo Red (Thermo Fisher Scientific) were reconstituted in PBS at 2 mg/ml. *A. aegypti* and *C. lectularius* were injected with 0.4 and 1 μl of pHrodo Red *E. coli*, respectively. At 1 and 4 hours after challenge, each insect was injected with 16% formaldehyde, and the dorsal abdomen was dissected and mounted as described above. Insects that were not injected were used as negative controls. Each dorsal abdomen was visualized under bright-field and fluorescence illumination, and images were acquired as detailed above. All images within a Z-stack were combined into a focused image using the EDF function in NIS-Elements, and the pHrodo Red channel was exported in monochrome. This experiment was replicated in three to four insects per treatment group for each species.

Visualization and quantification of hemocytes and pathogens in surveyed insects

Each dissected dorsal and ventral abdomen from an infected insect was imaged under bright-field and fluorescence illumination as described above. Each side of the abdomen was first imaged under low magnification to examine the distribution of hemocytes and GFP–*E. coli* over the entire length of the heart or the ventral nerve cord. Then, a region of the heart—and specifically, a periostial region where the ostia were clearly visible—was examined under high magnification to more clearly visualize the aggregation pattern of both hemocytes and GFP–*E. coli*. When an abdomen was too long to fit in a single frame at the lowest magnification, multiple images along the abdomen were acquired, and the images were stitched together using Adobe Photoshop CC 2019 (San Jose, CA, USA).

The aggregation pattern of hemocytes and pathogens was determined by examining the overlay of three fluorescence channels—red for hemocytes, green for GFP–*E. coli*, and blue for cell nuclei—relative to the position of the heart, as identified in the Z-stacks by bright-field imaging and the cell nuclei fluorescence channel. The judgment of where immune responses occur was based primarily on the GFP–*E. coli* channel because hemocyte staining in insects collected in the wild is noisier and less efficient than in mosquitoes reared in our laboratory. For quantitative analysis of the distribution of GFP–*E. coli*, ImageJ was used to count the pixels that contained GFP–*E. coli* signal in EDF images of the entire dorsal and ventral abdomen (Fig. 4 and figs. S2 to S10). These pixels were defined as the pixels with intensities above the threshold that distinguished GFP emitted by *E. coli* from background fluorescence. Quantitative analyses measured two different types of fluorescence distribution. To create the graphs to the left of the fluorescence images in Fig. 4, images were collapsed along the insect's anterior-posterior axis such that the number of pixels within a horizontal row that had fluorescence intensity values above the threshold was counted, and the frequency of GFP–*E. coli* pixels was plotted along the width (laterally, from side to side) of the dorsal (blue line) and ventral (red line) abdomen, with the heart and ventral nerve cord on the horizontal midline of each graph. This informs about (i) the relative distribution of fluorescence in the dorsal and ventral sides and (ii) whether fluorescence is concentrated on the heart (blue line with peak in the center) or is evenly distributed throughout the abdomen (blue line with no peak in the center). The frequency distribution of *E. coli* in the dorsal and ventral abdomen was compared by two-sample Kolmogorov-Smirnov test in the R software. To create the graphs to the right of the fluorescence images in Fig. 4, images were collapsed along the insect's left-right (lateral) axis such that the number of pixels within a vertical column that had fluorescence intensity values above the threshold was counted, and the frequency of GFP–*E. coli* was plotted along the length of the dorsal abdomen, with the anterior of the abdomen on the left and the posterior on the right. Together with the leftmost graphs showing heart-associated aggregation, the rightmost graphs in Fig. 4 inform about whether the GFP–*E. coli* does not aggregate or aggregates (i) in foci at the periostial regions (vertical peaks with valleys), (ii) in both foci and also along the length of the heart (vertical peaks but no consistent valleys), or (iii) at the posterior of the heart (peaks only on the right). Last, the pictures of the whole insects shown in Fig. 4 were either taken by the authors or acquired from the public domain.

SUPPLEMENTARY MATERIALS

Supplementary material for this article is available at http://advances.sciencemag.org/cgi/content/full/6/48/eabb3164/DC1

View/request a protocol for this paper from *Bio-protocol*.

REFERENCES AND NOTES

1. J. D. Glenn, J. G. King, J. F. Hillyer, Structural mechanics of the mosquito heart and its function in bidirectional hemolymph transport. *J. Exp. Biol.* **213**, 541–550 (2010).
2. G. P. League, O. C. Onuh, J. F. Hillyer, Comparative structural and functional analysis of the larval and adult dorsal vessel and its role in hemolymph circulation in the mosquito *Anopheles gambiae*. *J. Exp. Biol.* **218**, 370–380 (2015).
3. W. K. Lee, J. J. Socha, Direct visualization of hemolymph flow in the heart of a grasshopper (*Schistocerca americana*). *BMC Physiol.* **9**, 2 (2009).
4. J. F. Hillyer, G. Pass, The insect circulatory system: Structure, function, and evolution. *Annu. Rev. Entomol.* **65**, 121–143 (2020).
5. C. S. Wirkner, M. Togel, G. Pass, The arthropod circulatory system, in *Arthropod Biology and Evolution*, A. Minelli, G. Boxshall, G. Fusco, Eds. (Springer, 2013), chap. 14, pp. 343–391.
6. L. C. Bartholomay, K. Michel, Mosquito immunobiology: The intersection of vector health and vector competence. *Annu. Rev. Entomol.* **63**, 145–167 (2018).
7. J. G. King, J. F. Hillyer, Infection-induced interaction between the mosquito circulatory and immune systems. *PLOS Pathog.* **8**, e1003058 (2012).
8. J. G. King, J. F. Hillyer, Spatial and temporal in vivo analysis of circulating and sessile immune cells in mosquitoes: Hemocyte mitosis following infection. *BMC Biol.* **11**, 55 (2013).
9. L. T. Sigle, J. F. Hillyer, Mosquito hemocytes preferentially aggregate and phagocytose pathogens in the periostial regions of the heart that experience the most hemolymph flow. *Dev. Comp. Immunol.* **55**, 90–101 (2016).
10. P. J. Delves, S. J. Martin, D. R. Burton, I. M. Roitt, The anatomy of the immune response, in *Roitt's Essential Immunology* (Blackwell Publishing Ltd., 2011), chap. 7, pp. 188–204.
11. Y. Yan, J. F. Hillyer, Complement-like proteins TEP1, TEP3 and TEP4 are positive regulators of periostial hemocyte aggregation in the mosquito *Anopheles gambiae*. *Insect Biochem. Mol. Biol.* **107**, 1–9 (2019).
12. L. T. Sigle, J. F. Hillyer, *Eater* and *draper* are involved in the periostial haemocyte immune response in the mosquito *Anopheles gambiae*. *Insect Mol. Biol.* **27**, 429–438 (2018).
13. D. Cevik, M. Acker, C. Michalski, J. R. Jacobs, Pericardin, a *Drosophila* collagen, facilitates accumulation of hemocytes at the heart. *Dev. Biol.* **454**, 52–65 (2019).
14. R. da Silva, S. R. da Silva, A. B. Lange, The regulation of cardiac activity by nitric oxide (NO) in the Vietnamese stick insect, *Baculum extradentatum*. *Cell. Signal.* **24**, 1344–1350 (2012).
15. S. Ghosh, A. Singh, S. Mandal, L. Mandal, Active hematopoietic hubs in *Drosophila* adults generate hemocytes and contribute to immune response. *Dev. Cell* **33**, 478–488 (2015).
16. L. Horn, J. Leips, M. Starz-Gaiano, Phagocytic ability declines with age in adult *Drosophila* hemocytes. *Aging Cell* **13**, 719–728 (2014).

17. M. F. Pereira, C. C. Rossi, M. V. de Queiroz, G. F. Martins, C. Isaac, J. T. Bosse, Y. Li, B. W. Wren, V. S. Terra, J. Cuccui, P. R. Langford, D. M. Bazzolli, *Galleria mellonella* is an effective model to study *Actinobacillus pleuropneumoniae* infection. *Microbiology* **161**, 387–400 (2015).
18. B. Misof, S. Liu, K. Meusemann, R. S. Peters, A. Donath, C. Mayer, P. B. Frandsen, J. Ware, T. Flouri, R. G. Beutel, O. Niehuis, M. Petersen, F. Izquierdo-Carrasco, T. Wappler, J. Rust, A. J. Aberer, U. Aspock, H. Aspock, D. Bartel, A. Blanke, S. Berger, A. Bohm, T. R. Buckley, B. Calcott, J. Chen, F. Friedrich, M. Fukui, M. Fujita, C. Greve, P. Grobe, S. Gu, Y. Huang, L. S. Jermiin, A. Y. Kawahara, L. Krogmann, M. Kubiak, R. Lanfear, H. Letsch, Y. Li, Z. Li, J. Li, H. Lu, R. Machida, Y. Mashimo, P. Kapli, D. D. McKenna, G. Meng, Y. Nakagaki, J. L. Navarrete-Heredia, M. Ott, Y. Ou, G. Pass, L. Podsiadlowski, H. Pohl, B. M. von Reumont, K. Schutte, K. Sekiya, S. Shimizu, A. Slipinski, A. Stamatakis, W. Song, X. Su, N. U. Szucsich, M. Tan, X. Tan, M. Tang, J. Tang, G. Timelthaler, S. Tomizuka, M. Trautwein, X. Tong, T. Uchifune, M. G. Walzl, B. M. Wiegmann, J. Wilbrandt, B. Wipfler, T. K. Wong, Q. Wu, G. Wu, Y. Xie, S. Yang, Q. Yang, D. K. Yeates, K. Yoshizawa, Q. Zhang, R. Zhang, W. Zhang, Y. Zhang, J. Zhao, C. Zhou, L. Zhou, T. Ziesmann, S. Zou, Y. Li, X. Xu, Y. Zhang, H. Yang, J. Wang, J. Wang, K. M. Kjer, X. Zhou, Phylogenomics resolves the timing and pattern of insect evolution. *Science* **346**, 763–767 (2014).
19. S. Hernandez-Martinez, M. Sanchez-Zavaleta, K. Brito, A. Herrera-Ortiz, S. Ons, F. G. Noriega, Allatotropin: A pleiotropic neuropeptide that elicits mosquito immune responses. *PLOS ONE* **12**, e0175759 (2017).
20. E. M. Hystad, H. Salmela, G. V. Amdam, D. Munch, Hemocyte-mediated phagocytosis differs between honey bee (*Apis mellifera*) worker castes. *PLOS ONE* **12**, e0184108 (2017).
21. L. T. Sigle, J. F. Hillyer, Mosquito hemocytes associate with circulatory structures that support intracardiac retrograde hemolymph flow. *Front. Physiol.* **9**, 1187 (2018).
22. R. G. Chiang, J. A. Chiang, K. G. Davey, Morphology of the dorsal vessel in the abdomen of the blood-feeding insect *Rhodnius prolixus*. *J. Morphol.* **204**, 9–23 (1990).
23. T. A. Woolley, The circulatory system of the box elder bug *Leptocoris trivittatus* (Say). *Am Midl Nat* **46**, 634–639 (1951).
24. J. W. Andereck, J. G. King, J. F. Hillyer, Contraction of the ventral abdomen potentiates extracardiac retrograde hemolymph propulsion in the mosquito hemocoel. *PLoS One* **5**, e12943 (2010).
25. G. Pass, B. Gereben-Krenn, M. Merl, J. Plant, N. U. Szucsich, M. Tögel, Phylogenetic relationships of the orders in Hexapoda: Contributions from the circulatory organs for a morphological data matrix. *Arthropod. Syst. Phylo.* **64**, 165–203 (2006).
26. W. L. Nutting, A comparative anatomical study of the heart and accessory structures of the orthopteroid insects. *J. Morphol.* **89**, 501–597 (1951).
27. G. P. League, J. F. Hillyer, Functional integration of the circulatory, immune, and respiratory systems in mosquito larvae: Pathogen killing in the hemocyte-rich tracheal tufts. *BMC Biol.* **14**, 78 (2016).
28. T. Gopel, C. S. Wirkner, Morphological description, character conceptualization and the reconstruction of ancestral states exemplified by the evolution of arthropod hearts. *PLOS ONE* **13**, e0201702 (2018).
29. J. F. Hillyer, Insect immunology and hematopoiesis. *Dev. Comp. Immunol.* **58**, 102–118 (2016).
30. C. Kocks, J. H. Cho, N. Nehme, J. Ulvila, A. M. Pearson, M. Meister, C. Strom, S. L. Conto, C. Hetru, L. M. Stuart, T. Stehle, J. A. Hoffmann, J. M. Reichhart, D. Ferrandon, M. Ramet, R. A. Ezekowitz, Eater, a transmembrane protein mediating phagocytosis of bacterial pathogens in *Drosophila*. *Cell* **123**, 335–346 (2005).
31. I. Matetovici, J. Van Den Abbeele, Thioester-containing proteins in the tsetse fly (*Glossina*) and their response to trypanosome infection. *Insect Mol. Biol.* **27**, 414–428 (2018).
32. K. Somogyi, B. Sipos, Z. Penzes, E. Kurucz, J. Zsamboki, D. Hultmark, I. Ando, Evolution of genes and repeats in the Nimrod superfamily. *Mol. Biol. Evol.* **25**, 2337–2347 (2008).
33. J. F. Hillyer, Insect heart rhythmicity is modulated by evolutionarily conserved neuropeptides and neurotransmitters. *Curr Opin Insect Sci* **29**, 41–48 (2018).
34. K. E. Broderick, J. Feala, A. McCulloch, G. Paternostro, V. S. Sharma, R. B. Pilz, G. R. Boss, The nitric oxide scavenger cobinamide profoundly improves survival in a *Drosophila melanogaster* model of bacterial sepsis. *FASEB J.* **20**, 1865–1873 (2006).
35. T. Y. Estevez-Lao, L. T. Sigle, S. N. Gomez, J. F. Hillyer, Nitric oxide produced by periostial hemocytes modulates the bacterial infection induced reduction of the mosquito heart rate. *J. Exp. Biol.* **223**, jeb225821 (2020).
36. S. Smiljic, V. Nestorovic, S. Savic, Modulatory role of nitric oxide in cardiac performance. *Med. Pregl.* **67**, 345–352 (2014).
37. C. Bogdan, Nitric oxide synthase in innate and adaptive immunity: An update. *Trends Immunol.* **36**, 161–178 (2015).
38. D. A. Legg, M. D. Sutton, G. D. Edgecombe, Arthropod fossil data increase congruence of morphological and molecular phylogenies. *Nat. Commun.* **4**, 2485 (2013).
39. J. F. Harrison, Handling and use of oxygen by Pancrustaceans: Conserved patterns and the evolution of respiratory structures. *Integr. Comp. Biol.* **55**, 802–815 (2015).
40. J. F. Hillyer, Integrated immune and cardiovascular function in Pancrustacea: Lessons from the insects. *Integr. Comp. Biol.* **55**, 843–855 (2015).
41. J. R. Factor, M. Naar, The digestive system of the lobster, *Homarus americanus*: II. Terminal hepatic arterioles of the digestive gland. *J. Morphol.* **206**, 283–291 (1990).
42. P. T. Johnson, Bacterial infection in the blue crab, *Callinectes sapidus*: Course of infection and histopathology. *J. Invertebr. Pathol.* **28**, 25–36 (1976).
43. E. Sagrista, M. Durfort, Ultrastructural study of hemocytes and phagocytes associated with hemolymphatic vessels in the hepatopancreas of *Palaemonetes zariquieyi* (Crustacea, Decapoda). *J. Morphol.* **206**, 173–180 (1990).
44. K. Koiwai, H. Kondo, I. Hirono, The immune functions of sessile hemocytes in three organs of kuruma shrimp *Marsupenaeus japonicus* differ from those of circulating hemocytes. *Fish Shellfish Immunol.* **78**, 109–113 (2018).
45. L. Rusaini, Insight into the lymphoid organ of penaeid prawns: A review. *Fish Shellfish Immunol.* **29**, 367–377 (2010).
46. E. R. Eaton, K. Kaufman, *Kaufman Field Guide to Insects of North America* (Houghton Mifflin Company, 2007), pp. 392.
47. L. T. Wasserthal, *Drosophila* flies combine periodic heartbeat reversal with a circulation in the anterior body mediated by a newly discovered anterior pair of ostial valves and 'venous' channels. *J. Exp. Biol.* **210**, 3707–3719 (2007).

Acknowledgments: We thank P. Abbot, A. Rokas, S. Williams, and A. de Sá Nunes for commenting on this manuscript. We thank L. Jabbur, J. Sears, and M. Tackenberg for useful discussions and our friends and colleagues that assisted in insect collection (see the Supplementary Materials). **Funding:** This research was funded by NSF grants IOS-1456844 and IOS-1949145. **Author contributions:** Methodology, validation, analysis, resources, writing, and visualization: Y.Y. and J.F.H. Investigation: Y.Y. Conceptualization, supervision, project administration, and funding acquisition: J.F.H. **Competing interests:** The authors declare that they have no competing interests. **Data and materials availability:** All data needed to evaluate the conclusions in the paper are present in the paper and/or the Supplementary Materials. Additional data related to this paper may be requested from the authors.

Submitted 14 February 2020
Accepted 9 October 2020
Published 25 November 2020
10.1126/sciadv.abb3164

Citation: Y. Yan, J. F. Hillyer, The immune and circulatory systems are functionally integrated across insect evolution. *Sci. Adv.* **6**, eabb3164 (2020).

Science Advances
AAAS

advances.sciencemag.org/cgi/content/full/6/48/eabb3164/DC1

Supplementary Materials for

The immune and circulatory systems are functionally integrated across insect evolution

Yan Yan and Julián F. Hillyer*

*Corresponding author. Email: julian.hillyer@vanderbilt.edu

Published 25 November 2020, *Sci. Adv.* **6**, eabb3164 (2020)
DOI: 10.1126/sciadv.abb3164

This PDF file includes:

Figs. S1 to S10
Table S1

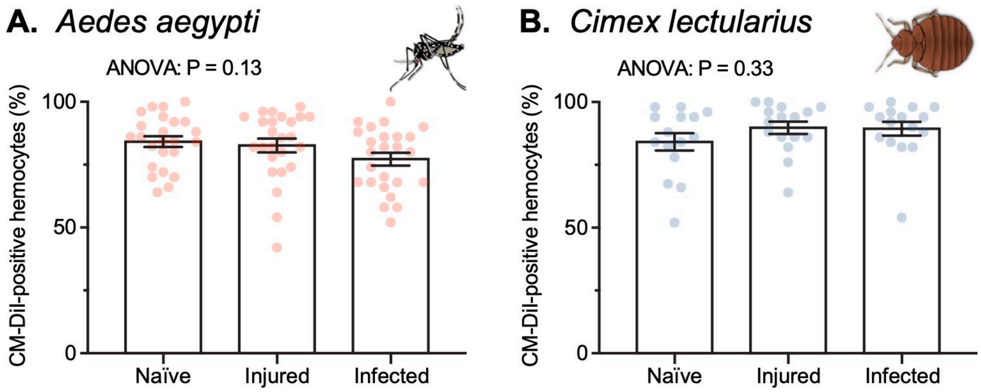

Fig. S1. The efficiency of Vybrant CM-DiI staining of hemocytes in *Aedes aegypti* and *Cimex lectularius*. Quantitative analysis of *in vivo* CM-DiI staining in perfused hemocytes from naïve, injured (LB) and *E. coli*-infected *Ae. aegypti* (**A**) and *C. lectularius* (**B**). Column heights mark the mean and the whiskers denote the standard error of the mean. Each circle represents the percentage of hemocytes that are positively stained by CM-DiI in an individual insect. The vast majority of hemocytes stain with CM-DiI.

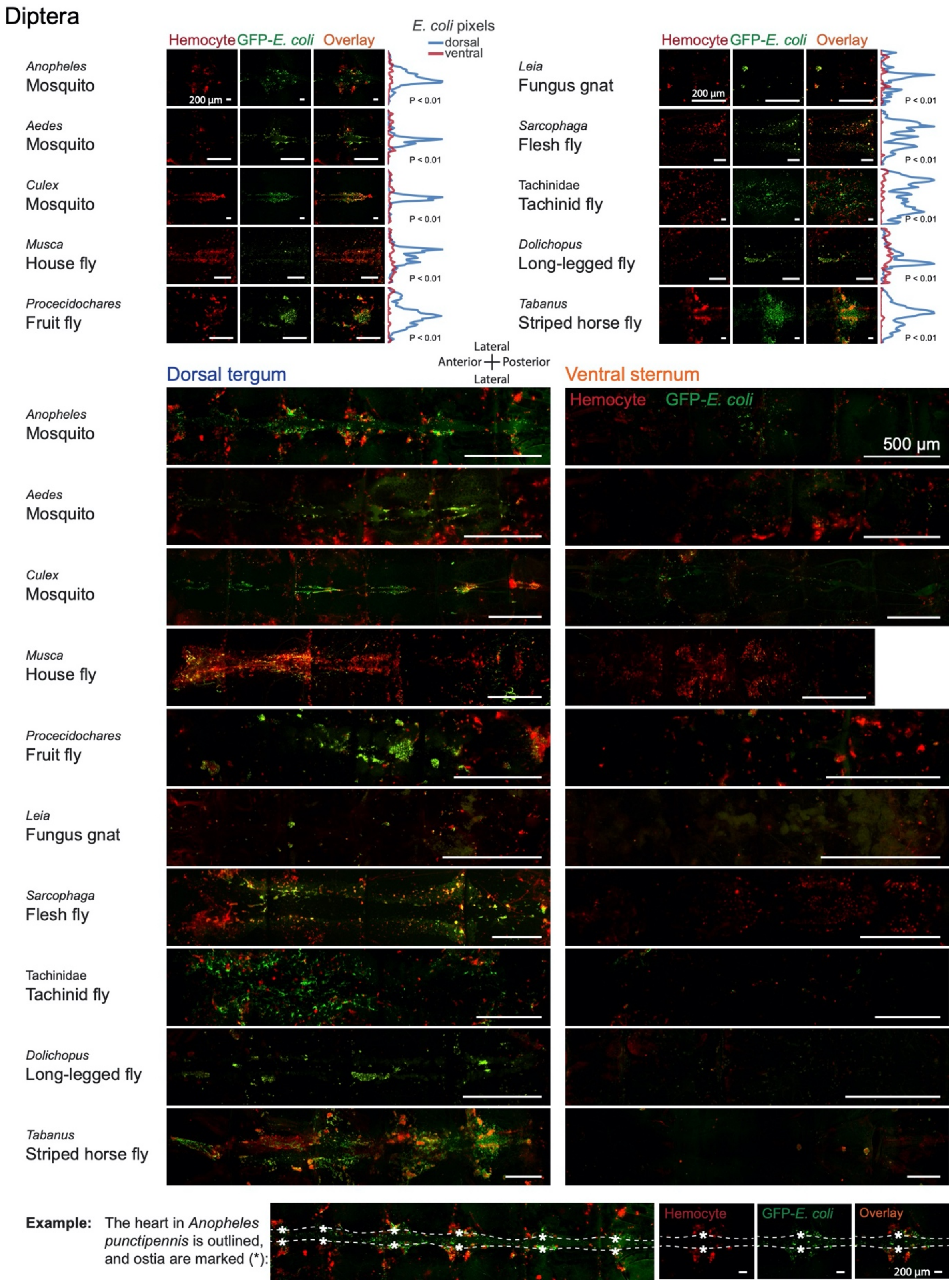

Fig. S2. The aggregation of hemocytes and pathogens on the heart of members of the order Diptera. Fluorescence microscopy images show one region of the heart (top section of the figure) and the entire dorsal and ventral abdomen (bottom section of the figure) in each insect. Graphs show quantification of GFP-*E. coli* pixel frequency along the width of the entire dorsal (blue line) and ventral (red line) abdomen. Hemocytes (red) and GFP-*E. coli* (green) distinctively aggregate and co-localize (overlay) on the heart – but not the surrounding tergum – and are largely absent in the ventral sternum.

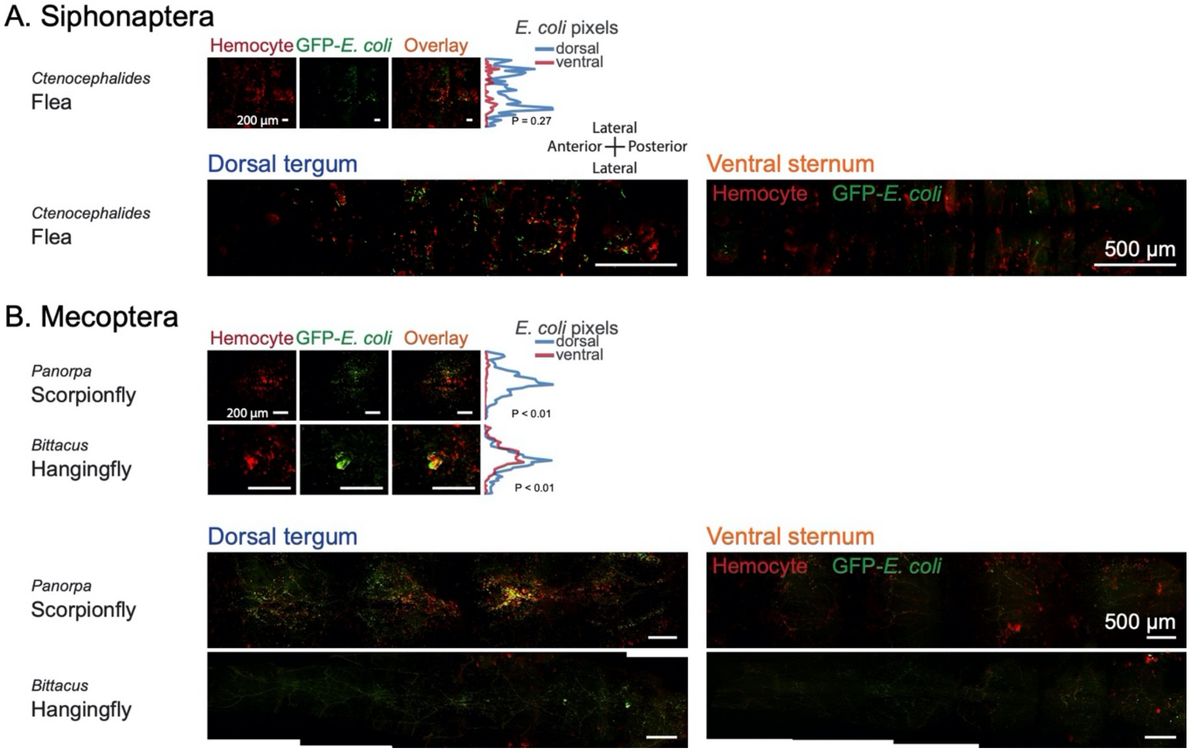

Fig. S3. The aggregation of hemocytes and pathogens on the heart of members of the orders Siphonaptera and Mecoptera. Fluorescence microscopy images show one region of the heart (top section of each panel) and the entire dorsal and ventral abdomen (bottom section of each panel) in each insect. Graphs show quantification of GFP-*E. coli* pixel frequency along the width of the entire dorsal (blue line) and ventral (red line) abdomen. In Siphonaptera (**A**), hemocytes (red) and GFP-*E. coli* (green) do not aggregate or co-localize (overlay) on the heart. In Mecoptera (**B**), hemocytes and GFP-*E. coli* distinctively aggregate and co-localize on the heart – but not the surrounding tergum – and are largely absent in the ventral sternum.

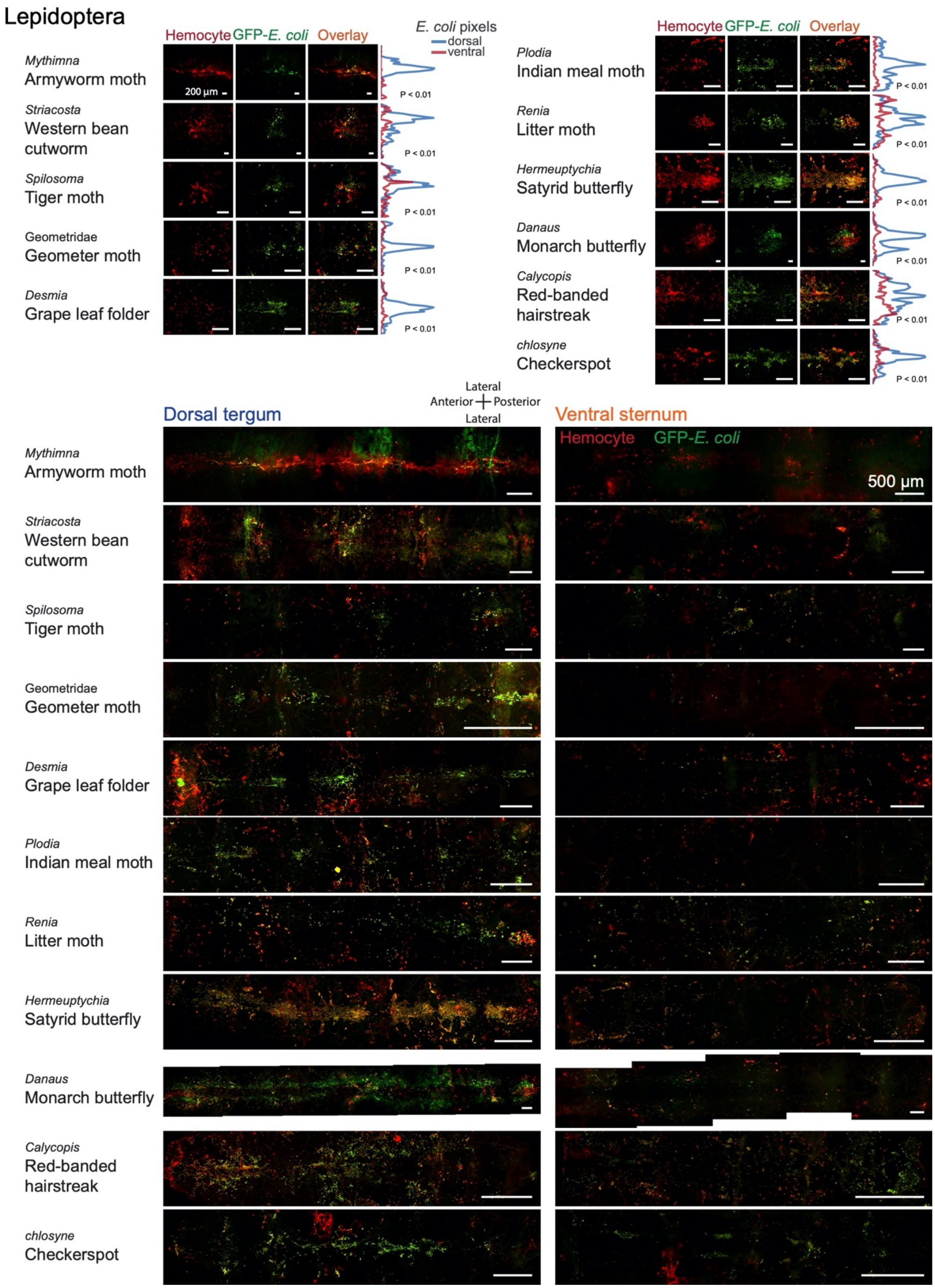

Fig. S4. The aggregation of hemocytes and pathogens on the heart of members of the order Lepidoptera. Fluorescence microscopy images show one region of the heart (top section of the figure) and the entire dorsal and ventral abdomen (bottom section of the figure) in each insect. Graphs show quantification of GFP-*E. coli* pixel frequency along the width of the entire dorsal (blue line) and ventral (red line) abdomen. Hemocytes (red) and GFP-*E. coli* (green) distinctively aggregate and co-localize (overlay) on the heart – but not the surrounding tergum – and are largely absent in the ventral sternum.

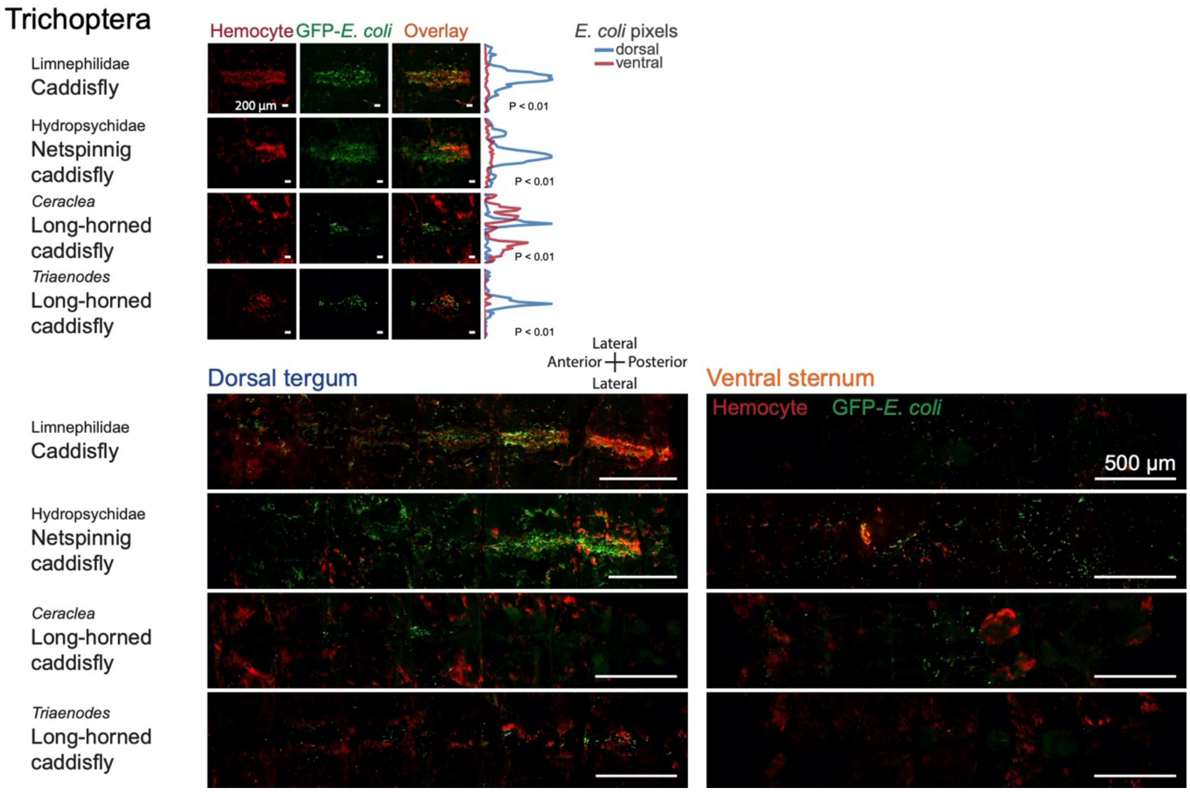

Fig. S5. The aggregation of hemocytes and pathogens on the heart of members of the order Trichoptera. Fluorescence microscopy images show one region of the heart (top section of the figure) and the entire dorsal and ventral abdomen (bottom section of the figure) in each insect. Graphs show quantification of GFP-*E. coli* pixel frequency along the width of the entire dorsal (blue line) and ventral (red line) abdomen. Hemocytes (red) and GFP-*E. coli* (green) distinctively aggregate and co-localize (overlay) on the heart – but not the surrounding tergum – and are largely absent in the ventral sternum.

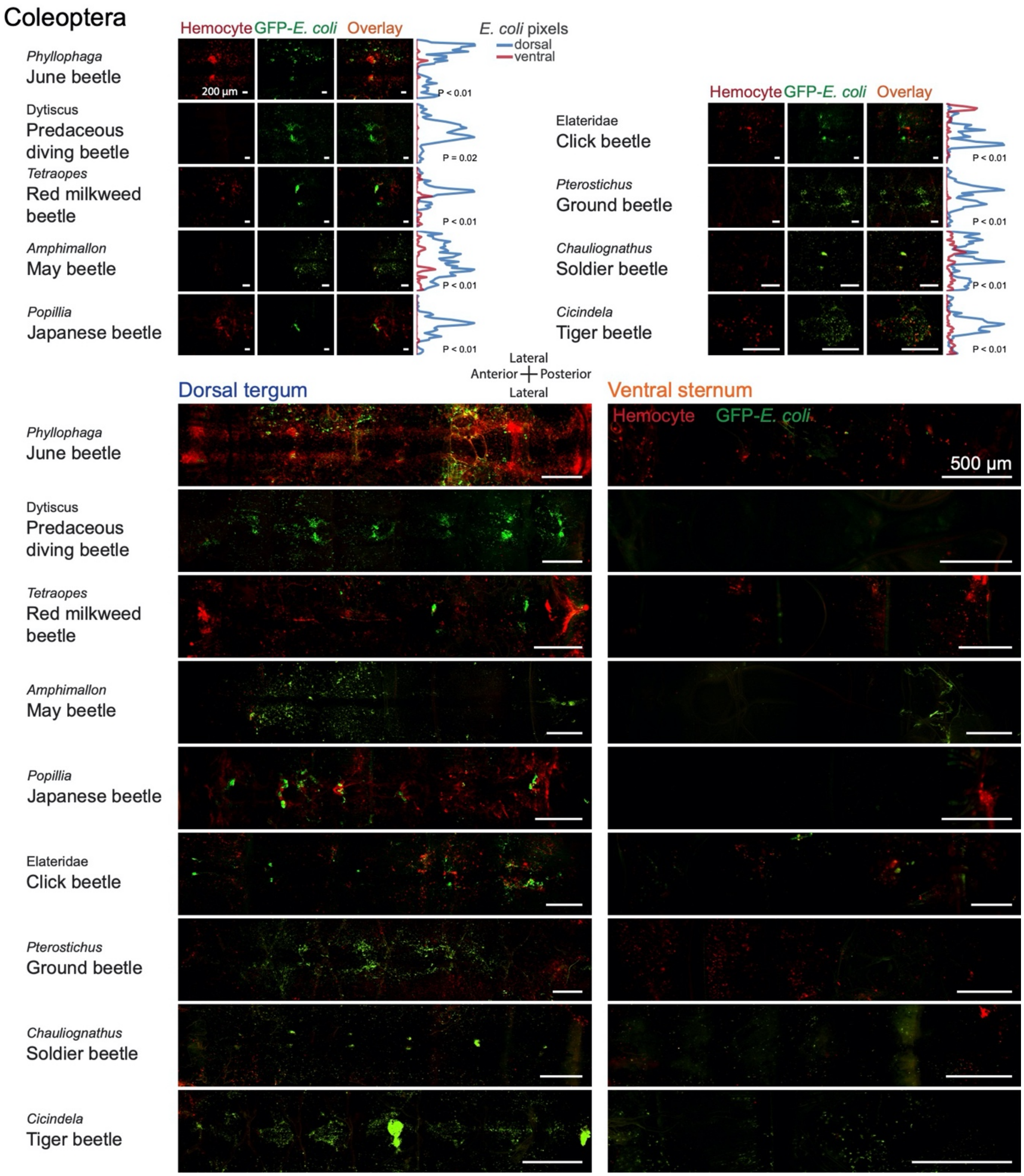

Fig. S6. The aggregation of hemocytes and pathogens on the heart of members of the order Coleoptera. Fluorescence microscopy images show one region of the heart (top section of the figure) and the entire dorsal and ventral abdomen (bottom section of the figure) in each insect. Graphs show quantification of GFP-*E. coli* pixel frequency along the width of the entire dorsal (blue line) and ventral (red line) abdomen. Hemocytes (red) and GFP-*E. coli* (green) distinctively aggregate and co-localize (overlay) on the heart – but not the surrounding tergum – and are largely absent in the ventral sternum.

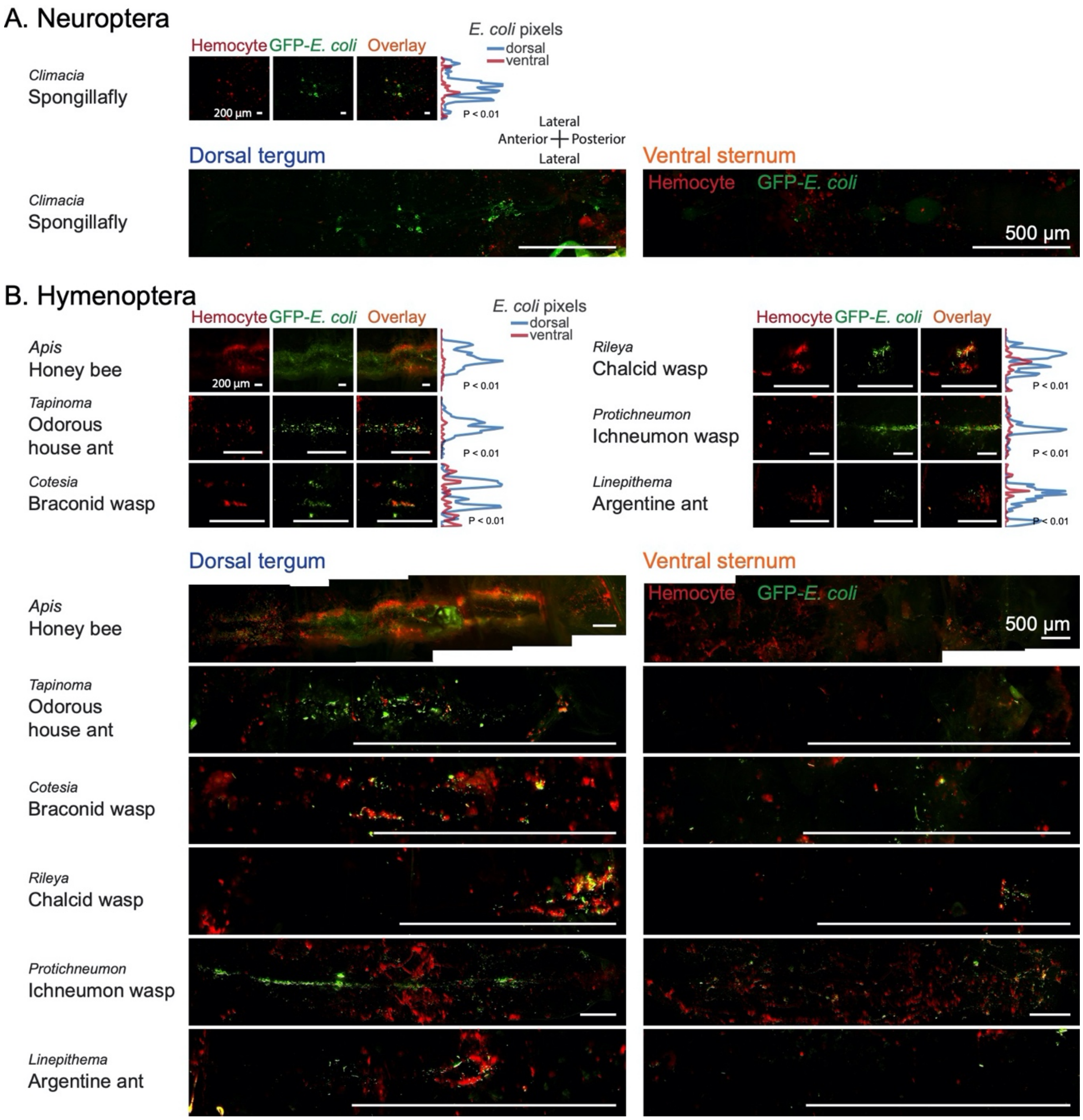

Fig. S7. The aggregation of hemocytes and pathogens on the heart of members of the orders Neuroptera and Hymenoptera. Fluorescence microscopy images show one region of the heart (top section of each panel) and the entire dorsal and ventral abdomen (bottom section of each panel) in each insect. Graphs show quantification of GFP-*E. coli* pixel frequency along the width of the entire dorsal (blue line) and ventral (red line) abdomen. In both Neuroptera (**A**) and Hymenoptera (**B**), hemocytes (red) and GFP-*E. coli* (green) distinctively aggregate and co-localize (overlay) on the heart – but not the surrounding tergum – and are largely absent in the ventral sternum.

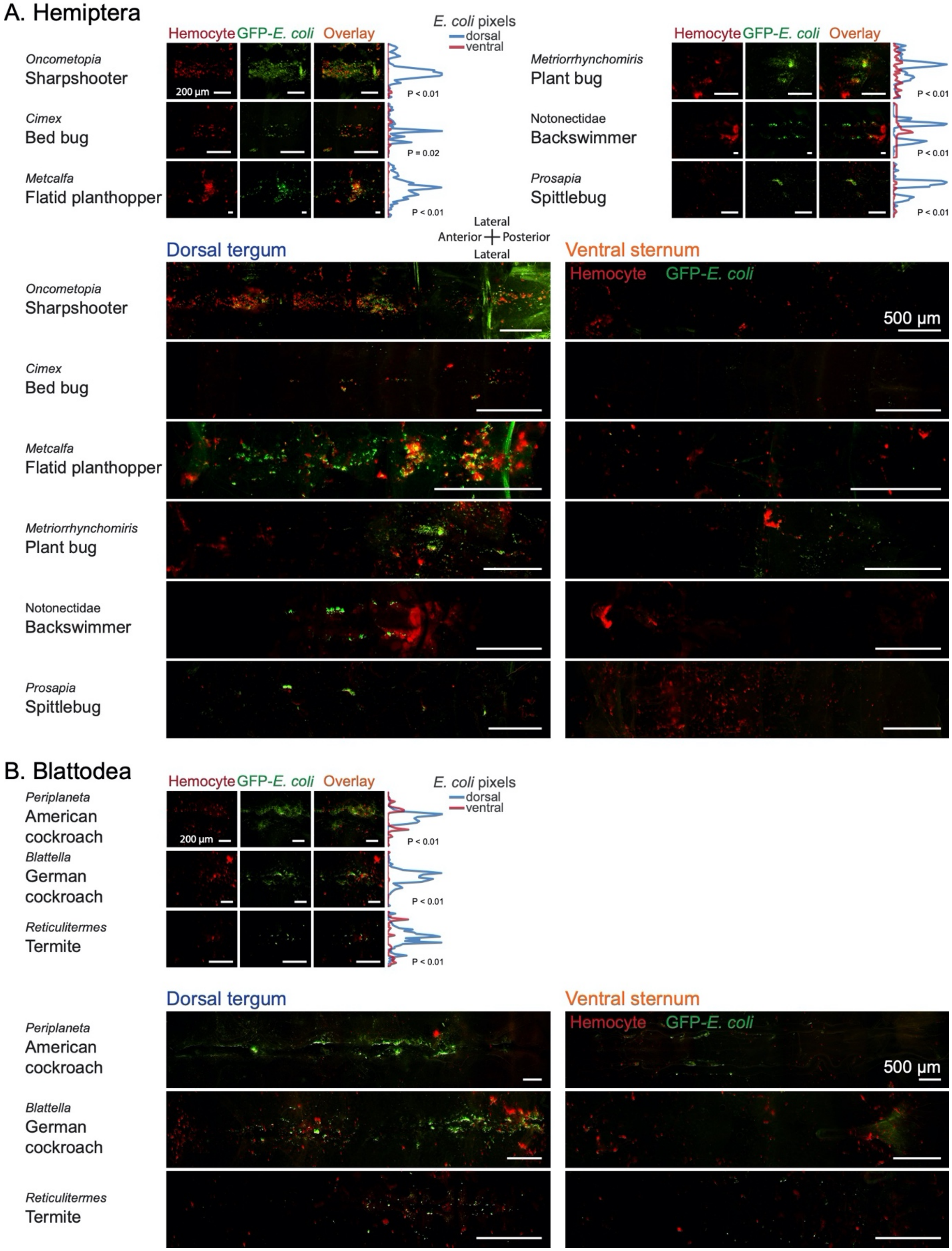

Fig. S8. The aggregation of hemocytes and pathogens on the heart of members of the orders Hemiptera and Blattodea. Fluorescence microscopy images show one region of the heart (top section of each panel) and the entire dorsal and ventral abdomen (bottom section of each panel) in each insect. Graphs show quantification of GFP-*E. coli* pixel frequency along the width of the entire dorsal (blue line) and ventral (red line) abdomen. In both Hemiptera (**A**) and Blattodea (**B**), hemocytes (red) and GFP-*E. coli* (green) distinctively aggregate and co-localize (overlay) on the heart – but not the surrounding tergum – and are largely absent in the ventral sternum.

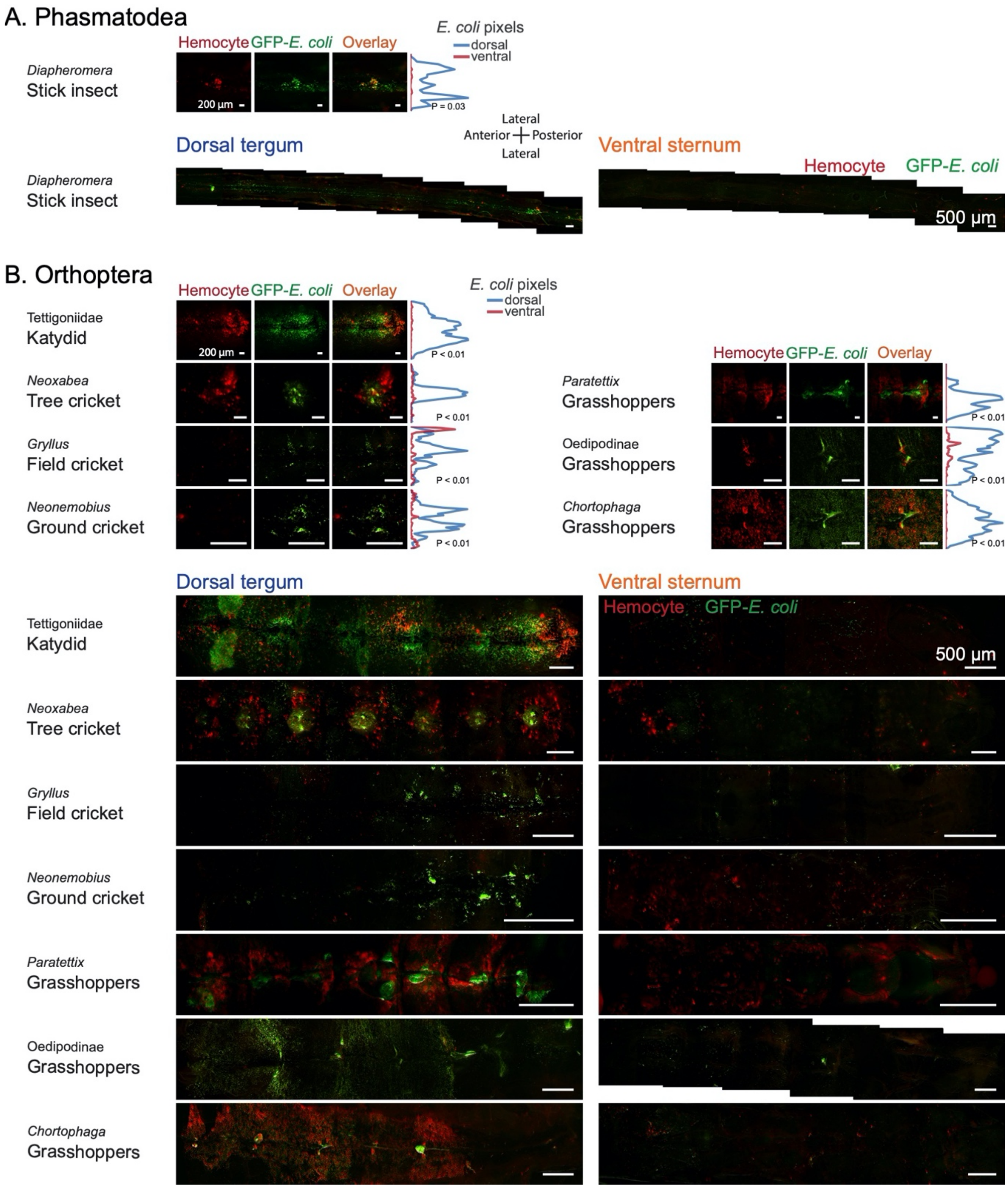

Fig. S9. The aggregation of hemocytes and pathogens on the heart of members of the orders Phasmatodea and Orthoptera. Fluorescence microscopy images show one region of the heart (top section of each panel) and the entire dorsal and ventral abdomen (bottom section of each panel) in each insect. Graphs show quantification of GFP-*E. coli* pixel frequency along the width of the entire dorsal (blue line) and ventral (red line) abdomen. In both Phasmatodea (**A**) and Orthoptera (**B**), hemocytes (red) and GFP-*E. coli* (green) distinctively aggregate and co-localize (overlay) on the heart – but not the surrounding tergum – and are largely absent in the ventral sternum.

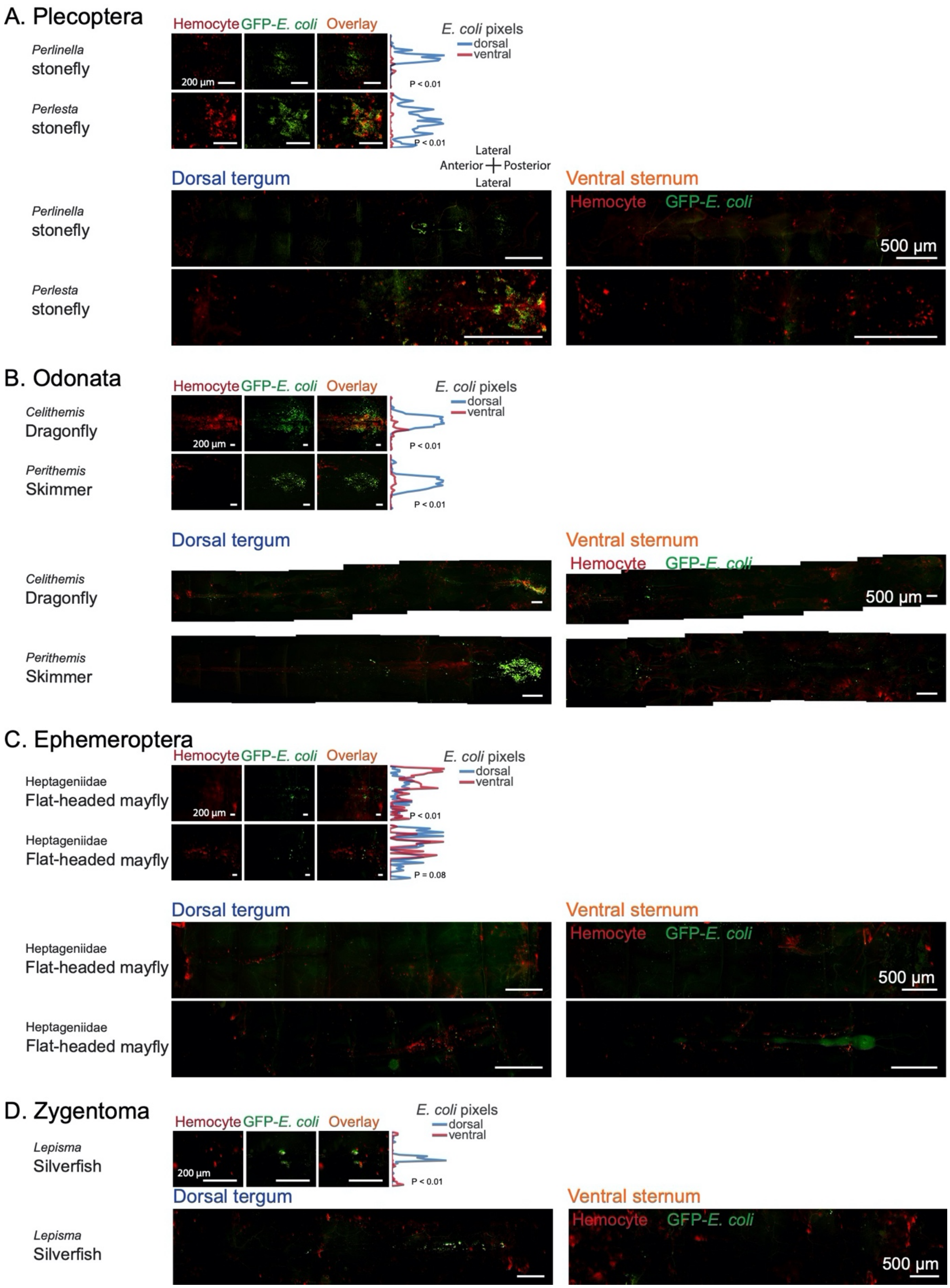

Fig. S10. The aggregation of hemocytes and pathogens on the heart of members of the orders Plecoptera, Odonata, Ephemeroptera and Zygentoma. Fluorescence microscopy images show one region of the heart (top section of each panel) and the entire dorsal and ventral abdomen (bottom section of each panel) in each insect. Graphs show quantification of GFP-*E. coli* pixel frequency along the width of the entire dorsal (blue line) and ventral (red line) abdomen. In Plecoptera (**A**), Odonata (**B**) and Zygentoma (**D**), hemocytes (red) and GFP-*E. coli* (green) distinctively aggregate and co-localize (overlay) on the posterior end of the heart – but not the surrounding tergum – and are largely absent in the ventral sternum. In Ephemeroptera (**C**), hemocytes and GFP-*E. coli* do not aggregate or co-localize on the heart.

Table S1. Detailed information on the insects used in this study.

Order	Family	Species	Common name	Location collected	Date of collection	Collection method	Collector[a]	Volume Injected (nL)	Number of *E. coli* injected	Incubation after infection
Zygentoma	Lepismatidae	*Lepisma saccharina*	Silverfish	Mulberry way, Nashville, TN	3/21/2019	trap	YY	1497	330903	1 hour
Ephemeroptera	Heptageniidae	*Leucrocuta* sp.	Mayfly	Mulberry way, Nashville, TN	7/31/2019	light trap	YY	311	215798	1 hour
Ephemeroptera	Heptageniidae	Unidentified	Flat-headed mayfly	Mulberry way, Nashville, TN	6/24/2019	light trap	YY	200	106200	4 hours
Odonata	Libellulidae	*Celithemis elisa*	Dragonfly	Leopold, IN	7/28/2019	sweep net	YY	6141	4722429	1 hour
Odonata	Libellulidae	*Perithemis tenera*	Skimmer	Willow Pond, Nashville, TN	7/7/2018	sweep net	YY, LJ	4140	1349640	1 hour
Plecoptera	Perlidae	*Perlinella* sp.	Stonefly	Hidden Lake Trail, Harpeth River State Park, Nashville, TN	6/9/2018	sweep net	YY, LJ, JS, PR, MT	3795	2819685	1 hour
Plecoptera	Perlidae	*Perlesta* sp.	Stonefly	Bellevue, Nashville, TN	7/19/2019	light trap	LJ	759	53130	1 hour
Orthoptera	Tettigoniidae	Unidentified	Katydid	Mulberry way, Nashville, TN	7/30/2019	light trap	YY	20100	10311300	1 hour
Orthoptera	Gryllidae	*Neoxabea* sp.	Tree cricket	Mulberry way, Nashville, TN	7/21/2019	sweep net	YY	4830	1197840	1 hour
Orthoptera	Gryllidae	*Gryllus* sp.	Field cricket	Deer Trail, Long Hunter State Park, TN	4/28/2019	sweep net	YY, LJ, PR, EH, MW	15000	14520000	4 hours
Orthoptera	Gryllidae	*Neonemobius* sp.	Ground cricket	Willow Pond, Nashville, TN	7/7/2018	sweep net	YY, LJ	3126	3344499	1 hour
Orthoptera	Tetrigidae	*Paratettix* sp.	Grasshopper	Willow Pond, Nashville, TN	5/25/2019	sweep net	YY, LJ, JC, DG	3933	3028410	4 hours
Orthoptera	Acrididae	Unidentified	Grasshopper	Deer Trail, Long Hunter State Park, TN	4/28/2019	sweep net	YY, LJ, PR, EH, MW	30000	29460000	4 hours
Orthoptera	Acrididae	*Chortophaga* sp.	Grasshopper	Hidden Lake Trail, Harpeth River State Park, Nashville, TN	6/9/2018	sweep net	YY, LJ, JS, PR, MT	17733	13175619	1 hour
Phasmatodea	Diapheromeridae	*Diapheromera femorata*	Walking stick	Bellevue, Nashville, TN	8/21/2019	sweep net	MGG	15870	6824100	1 hour
Blattodea	Blattidae	*Periplaneta americana*	American cockroach	Purdue University, West Lafayette, IN	5/6/2019	lab colony	GB	43263	29245788	4 hours
Blattodea	Ectobiidae	*Blattella germanica*	German cockroach	Purdue University, West Lafayette, IN	5/6/2019	lab colony	GB	5590	3778840	4 hours
Blattodea	Rhinotermitidae	*Reticulitermes flavipes*	Termite	Purdue University, West Lafayette, IN	5/6/2019	lab colony	GB	69	66171	4 hours
Hemiptera	Cicadellidae	*Oncometopia* sp.	Sharpshooter	Mulberry way, Nashville, TN, USA	5/24/2018	sweep net	YY	3588	2619240	1 hour
Hemiptera	Cimicidae	*Cimex lectularius*	Bed bug	Purdue University, West Lafayette, IN	5/6/2019	lab colony	GB, AG	276	186576	4 hours
Hemiptera	Flatidae	*Metcalfa* sp.	Flatid planthopper	Mulberry way, Nashville, TN	8/4/2019	light trap	YY	725	607131	1 hour
Hemiptera	Miridae	*Metriorrhynchomiris* sp.	Plant bug	Gossett Tract, Harpeth River State Park, Kingston Springs, TN	5/18/2019	sweep net	YY, SW, MT, MGG	828	355212	4 hours
Hemiptera	Notonectidae	Unidentified	Backswimmer	West Lafayette, IN	6/29/2019	light trap	SW	1380	1188180	4 hours
Hemiptera	Cercopidae	*Prosapia bicincta*	Spittlebug	Willow Pond, Nashville, TN	7/7/2018	sweep net	YY, LJ	2760	2969760	1 hour
Hymenoptera	Apidae	*Apis mellifera*	Honeybee	Vanderbilt University Campus, Nashville, TN	5/23/2018	sweep net	LJ	18561	13549530	1 hour

Hymenoptera	Formicidae	*Tapinoma sessile*	Odorous house ant	Purdue University, West Lafayette, IN	5/6/2019	lab colony	GB	40	37360	4 hours
Hymenoptera	Braconidae	*Cotesia* sp.	Braconid wasp	Nolensville pike, TN (emerged from hornworm caterpillar)	7/18/2019	by hand	PR	46	9062	1 hour
Hymenoptera	Eurytomidae	*Rileya* sp.	Chalcid wasp	Willow Pond, Nashville, TN	5/25/2019	sweep net	YY, LJ, JC, DG	27	20790	4 hours
Hymenoptera	Ichneumonidae	*Protichneumon grandis*	Ichneumon wasp	Willow Pond, Nashville, TN	7/7/2018	sweep net	YY, LJ	4009	3700215	1 hour
Hymenoptera	Formicidae	*Linepithema humile*	Argentine ant	Purdue University, West Lafayette, IN	5/6/2019	lab colony	GB	40	37360	4 hours
Neuroptera	Sisyridae	*Climacia* sp.	Spongillafly	Mulberry way, Nashville, TN	7/9/2019	light trap	YY	173	132825	1 hour
Coleoptera	Scarabaeidae	*Phyllophaga* sp.	June beetle	Mulberry way, Nashville, TN	6/18/2019	light trap	YY	11730	3190560	4 hours
Coleoptera	Dytiscus	Unidentified	Predaceous diving beetle	West Lafayette, IN	7/15/2019	light trap	SW	4913	4116926	1 hour
Coleoptera	Cerambycidae	*Tetraopes* sp.	Red milkweed beetle	West Lafayette, IN	7/21/2019	sweep net	SW	8280	6375600	1 hour
Coleoptera	Scarabaeidae	*Amphimallon* sp.	May beetle	Bellevue, Nashville, TN	4/21/2019	light trap	JH	9522	9998100	1 hour
Coleoptera	Scarabaeidae	*Popillia japonica*	Japanese beetle	Vanderbilt University Campus, Nashville, TN	6/17/2019	sweep net	YY	6486	252954	4 hours
Coleoptera	Elateridae	Unidentified	Click beetle	Mulberry way, Nashville, TN	6/18/2019	light trap	YY	5106	3497610	4 hours
Coleoptera	Carabidae	*Pterostichus* sp.	Ground beetle	Bellevue, Nashville, TN	6/8/2019	trap	LJ	15870	11934240	1 hour
Coleoptera	Cantharidae	*Chauliognathus marginatus*	Soldier beetle	Hidden Lake Trail, Harpeth River State Park, Nashville, TN	6/2/2018	sweep net	YY, LJ, JC, JS	3243	1563126	1 hour
Coleoptera	Carabidae	*Cicindela sexguttata*	Tiger beetle	Hidden Lake Trail, Harpeth River State Park, Nashville, TN	6/9/2018	sweep net	YY, LJ, JS, PR, MT	5382	3998826	1 hour
Trichoptera	Limnephilidae	Unidentified	Northern caddisfly	Mulberry way, Nashville, TN	7/28/2019	light trap	YY	276	212244	1 hour
Trichoptera	Hydropsychidae	Unidentified	Net-spinning caddisfly	Mulberry way, Nashville, TN	7/31/2019	light trap	YY	1297	901554	1 hour
Trichoptera	Leptoceridae	*Ceraclea* sp.	Long-horned caddisfly	Mulberry way, Nashville, TN	7/29/2019	light trap	YY	173	127995	1 hour
Trichoptera	Leptoceridae	*Triaenodes* sp.	Long-horned caddisfly	Mulberry way, Nashville, TN	7/10/2019	light trap	YY	235	66157	1 hour
Lepidoptera	Noctuidae	*Mythimna* sp.	Armyworm moth	Mulberry way, Nashville, TN	6/18/2019	light trap	YY	14490	3941280	4 hours
Lepidoptera	Noctuidae	*Striacosta albicosta*	Western bean cutworm	Cornfield, IN	7/11/2019	sweep net	SW	10557	2079729	1 hour
Lepidoptera	Erebidae	*Spilosoma* sp.	Tiger moth	Willow Pond, Nashville, TN	5/25/2019	sweep net	YY, LJ, JC, DG	5589	4303530	4 hours
Lepidoptera	Geometridae	Unidentified	Geometer moth	Deer Trail, Long Hunter State Park, Hermitage, TN	4/28/2019	sweep net	YY, LJ, PR, EH, MW	759	745338	4 hours
Lepidoptera	Crambidae	*Desmia* sp.	Grape leaf folder	Willow Pond, Nashville, TN	7/7/2018	sweep net	YY, LJ	2491	2680208	1 hour
Lepidoptera	Pyralidae	*Plodia interpunctella*	Indian meal moth	Purdue University, West Lafayette, IN	5/6/2019	lab colony	SW	552	395232	1 hour
Lepidoptera	Erebidae	*Renia* sp.	Litter moth	Gossett Tract, Harpeth River State Park, Kingston Springs, TN	5/18/2019	sweep net	YY, SW, MT, MGG	2484	1967328	4 hours
Lepidoptera	Nymphalidae	*Hermeuptychia* sp.	Satyrid butterfly	Willow Pond, Nashville, TN	7/1/2018	sweep net	YY, LJ	2491	3437442	1 hour
Lepidoptera	Nymphalidae	*Danaus plexippus*	Monarch butterfly	Leopold, IN	7/28/2019	sweep net	YY	45512	33769904	1 hour
Lepidoptera	Lycaenidae	*Calycopis* sp.	Red-banded hairstreak	Willow Pond, Nashville, TN	7/1/2018	sweep net	YY, LJ	1270	1752048	1 hour

Lepidoptera	Nymphalidae	*Chlosyne* sp.	Checkerspot	Willow Pond, Nashville, TN	7/1/2018	sweep net	YY, LJ	1608	2218626	1 hour
Mecoptera	Panorpidae	*Panorpa* sp.	Scorpionfly	Gossett Tract, Harpeth River State Park, Kingston Springs, TN	5/18/2019	sweep net	YY, SW, MT, MGG	2484	1967328	4 hours
Mecoptera	Bittacidae	*Bittacus* sp.	Hangingfly	Willow Pond, Nashville, TN	7/7/2018	sweep net	YY, LJ	1546	1545600	1 hour
Siphonaptera	Pulicidae	*Ctenocephalides felis*	Cat flea	Bellevue, Nashville, TN	7/13/2019	trap	LJ	69	18768	1 hour
Diptera	Culicidae	*Culex* sp.	Mosquito	Cheekwood Garden, Nashville, TN	5/17/2019	scooping	YY	207	80523	1 hour
Diptera	Culicidae	*Aedes albopictus*	Mosquito	Vanderbilt University Campus, Nashville, TN	7/21/2019	sweep net	YY, LJ	90	22246	1 hour
Diptera	Culicidae	*Anopheles punctipennis*	Mosquito	Mulberry way, Nashville, TN	8/15/2019	trap	YY	104	67068	1 hour
Diptera	Muscidae	*Musca domestica*	House fly	Belle Forest Cave, Bellevue, TN	5/12/2018	sweep net	YY, JS	235	142061	1 hour
Diptera	Tephritidae	*Procecidochares* sp.	Fruit fly	Willow Pond, Nashville, TN	5/25/2019	sweep net	YY, LJ, JC, DG	414	318780	4 hours
Diptera	Mycetophilidae	*Leia bivittate*	Fungus gnat	Hidden Lake Trail, Harpeth River State Park, Nashville, TN	6/9/2018	sweep net	YY, LJ, JS, PR, MT	173	129720	1 hour
Diptera	Sarcophagidae	*Sarcophaga* sp.	Flesh fly	Gossett Tract, Harpeth River State Park, Kingston Springs, TN	5/18/2019	sweep net	YY, SW, MT, MGG	1104	473616	4 hours
Diptera	Tachinidae	Unidentified	Tachinid fly	North Judson, IN (emerged from monarch caterpillar)	8/4/2019	by hand	SW	1201	1006103	1 hour
Diptera	Dolichopodidae	*Dolichopus* sp.	Long-legged fly	Hidden Lake Trail, Harpeth River State Park, Nashville, TN	6/9/2018	sweep net	YY, LJ, JS, PR, MT	676	508502	1 hour
Diptera	Tabanidae	*Tabanus* sp.	Striped horse fly	Leopold, IN	7/28/2019	sweep net	YY	2001	1538769	1 hour

[a] YY = Yan Yan; LJ = Luisa Jabbur; JS = Jacob Steenwyk; PR = Parker Rundstrom; MT = Michael Tackenberg; EH = Emily Hudson; MW = Matt Wilkins; JC = Justin Critchlow; DG = Destane Garrett; MGG = Manuel Giannoni Guzman; GB = Grzegorz Buczkowski; AG = Ameya Gondhalekar; SW = Scott Williams; JH = Julián Hillyer.